



Simulating energy and water balance with freezing and terrain effects

S. Endrizzi et al.

# GEOtop 2.0: simulating the combined energy and water balance at and below the land surface accounting for soil freezing, snow cover and terrain effects

S. Endrizzi<sup>1</sup>, S. Gruber<sup>2</sup>, M. Dall’Amico<sup>3</sup>, and R. Rigon<sup>4</sup>

<sup>1</sup>Department of Geography, University of Zurich, Winterthurerstrasse 190, 8057 Zurich, Switzerland

<sup>2</sup>Carleton University, Department of Geography and Environmental Studies, 1125 Colonel By Drive, Ottawa, ON K1S 5B6, Canada

<sup>3</sup>Mountain-eering GmbH, Siemensstrasse 19, 39100 Bozen, Italy

<sup>4</sup>Dipartimento di Ingegneria Civile, Ambientale e Meccanica e CUDAM, Università di Trento, Via Mesiano 77, 38123 Trento, Italy

Received: 4 October 2013 – Accepted: 21 October 2013 – Published: 3 December 2013

Correspondence to: S. Endrizzi (stefano.end@gmail.com)  
and M. Dall’Amico (matteo@mountain-eering.com)

Published by Copernicus Publications on behalf of the European Geosciences Union.

Title Page

Abstract

Introduction

Conclusions

References

Tables

Figures



Back

Close

Full Screen / Esc

Printer-friendly Version

Interactive Discussion



## Abstract

GEOtop is a small-scale grid-based simulator that represents the heat and water budgets at and below the soil surface. It represents the energy exchange with the atmosphere, considering the radiative and turbulent fluxes, and describes the three-dimensional subsurface water flow. Furthermore, it reproduces the highly non-linear interaction of the water and energy balance during soil freezing and thawing, and describes the temporal evolution of water and energy budgets in the snow cover and their effect on soil temperature.

Here, we describe the core components of GEOtop 2.0 and demonstrate its functioning. Based on a synthetic simulation, we show that the interaction of processes represented in GEOtop 2.0 can result in phenomena that are significant and relevant for applications involving permafrost and seasonally-frozen soils, both in high altitude and latitude regions.

## 1 Introduction

Frozen soil and snow cover interact in various ways with hydrology, climate, ecosystems and with human infrastructures. These natural systems are complex and characterised by many non-linear processes that operate and interact over different scales. Their mathematical representation and quantification is gaining in importance, especially in the light of global climate change. This importance derives on one hand from the requirement to study more and more complex systems, and, on the other hand, this representation of more complex systems can inform decisions about their simplification. The systems of equations required for representing such environments are often simplified by excluding processes that are considered less important for the problems addressed. Such an a priori exclusion, however, may not be quantitatively justified and mostly dictated by the need for mathematical tractability. Estimating the error inherent in model simplifications is therefore desirable for weighing the costs and benefits of differing options.

## Simulating energy and water balance with freezing and terrain effects

S. Endrizzi et al.

Title Page

Abstract

Introduction

Conclusions

References

Tables

Figures



Back

Close

Full Screen / Esc

Printer-friendly Version

Interactive Discussion







## Simulating energy and water balance with freezing and terrain effects

S. Endrizzi et al.

Title Page

Abstract

Introduction

Conclusions

References

Tables

Figures

⏪

⏩

◀

▶

Back

Close

Full Screen / Esc

Printer-friendly Version

Interactive Discussion

with a bulk method (Zanotti et al., 2004) and the surface energy balance, though complete in its components and accommodating complex terrain, was not numerically coupled to the soil heat equation. In GEOtop 2.0, soil freezing and thawing are represented, meteorological forcings are distributed, and channel routing is described as overland flow with the shallow water equation neglecting the inertia. The description of vegetation with a double-layer surface scheme in order to more accurately represent the heat and vapour exchanges of vegetation with the soil surface and the atmosphere has also been included in GEOtop and described in Endrizzi and Marsh (2010).

The core components of GEOtop, namely the soil volumetric system and the equations to be solved, the interaction with the atmosphere, the effects of complex terrain, the numerics, the representation of the snow cover, and the distribution of the meteorological data are here described. It is shown that the simulator produces plausible results in its major components. In addition, a simulation experiment is presented in order to demonstrate that the combination of terrain effects, energy and water balance produce unique results for different meteorological forcings, making an a priori exclusion of any of these processes difficult and providing one important rationale for developing and using a simulator such as GEOtop.

## 2 Volumetric system

The volumetric system consists of a soil volume of a user-specified uniform depth (typically a few metres to hundreds of metres) and is discretized in several layers parallel to the surface. Close to the surface the layers are usually prescribed thinner than at depth, as the gradients of temperature and water content resulting from the interaction with the atmosphere are stronger. The surface can be additionally discretized spatially using a regular square grid. Therefore, the elementary units, here referred to as “cells”, are given by the volumes resulting from the intersection of layers parallel to the surface with the columns defined in a direction normal to the surface.

The heat and water flow equations are not fully coupled numerically, but they are linked in a time-lagged manner (e.g., Panday and Huyakorn, 2004). This method allows keeping the complexity of the numerics moderate, while the equations are solved reasonably fast.

## 5 2.1 Heat equation

As explained in Appendix B, the system of equations that is solved is:

$$\frac{\partial U^{\text{ph}}}{\partial t} + \nabla \bullet \mathbf{G} + S_{\text{en}} - \rho_w [L_f + c_w(T - T_{\text{ref}})] S_w = 0 \quad (1)$$

where  $U^{\text{ph}}$  is the volumetric internal energy of soil ( $\text{Jm}^{-3}$ ) subject to phase change,  $t$  (s) time,  $\nabla \bullet$  the divergence operator,  $\mathbf{G}$  the heat conduction flux ( $\text{Wm}^{-2}$ ),  $S_{\text{en}}$  the sink term of energy losses ( $\text{Wm}^{-3}$ ),  $S_w$  the sink term of mass losses ( $\text{s}^{-1}$ ),  $L_f$  ( $\text{Jkg}^{-1}$ ) is the latent heat of fusion,  $\rho_w$  the density of liquid water in soil ( $\text{kgm}^{-3}$ ),  $T$  ( $^{\circ}\text{C}$ ) the soil temperature and  $T_{\text{ref}}$  ( $^{\circ}\text{C}$ ) the reference temperature at which the internal energy is calculated. Writing  $\mathbf{G}$  according to the Fourier's law and considering Eq. (B9), Eq. (1) becomes:

$$15 \frac{\partial U^{\text{ph}}}{\partial t} + \nabla \bullet (-\lambda_T \nabla T) + S_{\text{en}} - u_f S_w = 0 \quad (2)$$

where  $\lambda_T$  is the thermal conductivity ( $\text{Wm}^{-1}\text{K}^{-1}$ ). Equation (2) is numerically solved one-dimensionally neglecting the lateral gradients.

Since the total mass of water is kept constant and is given by the resolution of the water balance equation in time lagged manner, the unknown of Eq. (2) is  $T$ . However, the equation determines the mass that changes phase. Since ice has a lower density than liquid water, freezing would lead to unrealistically large gauge pressures that cannot be converted into an expansion of the soil matrix, due to the lack of a mechanical model. Therefore, similarly to Dall'Amico et al. (2011a), a rigid

soil scheme is assumed, which implies that no volume expansion during freezing is allowed, and the densities of ice and liquid water are equal, and set to  $1000 \text{ kg m}^{-3}$ .

The expression of  $dU^{\text{ph}}$ , defined in Eq. (B13), implies a proper description of soil freezing and thawing processes. Water phase change from liquid to solid state in the soil is not an isothermal process like in free-surface water (e.g., Wettlaufer and Worster, 2006). Rather, phase change occurs over a range of temperatures. Several authors (e.g., Spaans and Baker, 1996) have defined fixed relations between unfrozen water content and temperature, referred to as “freezing soil characteristic curve”. This is a simplification, since more complex behaviours have been observed (Koopmans and Miller, 1966). The ice volumetric content can then be calculated as the difference of total and unfrozen water contents. The definition of the freezing soil characteristic curve allows expressing  $dU^{\text{ph}}$  in the following way:

$$dU^{\text{ph}} = CdT + \rho_w [L_f + (c_w - c_i)(T - T_{\text{ref}})] d\theta_w^{\text{ph}} = C_a dT \quad (3)$$

where  $C$  is the volumetric heat capacity ( $\text{J m}^{-3} \text{K}^{-1}$ ) defined in Appendix B,  $c_i$  and  $c_w$  ( $\text{J kg}^{-1} \text{K}^{-1}$ ) are the specific thermal capacity of ice and liquid water, respectively, and  $C_a$  is referred to as apparent heat capacity, function of temperature, defined as:

$$C_a = C + \rho_w [L_f + (c_w - c_i)(T - T_{\text{ref}})] \frac{d\theta_w^{\text{ph}}}{dT} \quad (4)$$

The thermal conductivity ( $\lambda_T$ ) is a combination of the thermal conductivities of each component of the soil multiphase mixture ( $\lambda_{\text{sp}}$  for soil matrix,  $\lambda_i$  for ice,  $\lambda_w$  for liquid water, and  $\lambda_a$  for air). It is, therefore, a non-linear function of temperature, since the proportion of liquid water and ice contents depends on temperature. While a simple additive mixing law is exact for the heat capacity, the behaviour of a multiphase mixture concerning the thermal conductivity is much more complex. Several non-linear mixing laws have been proposed (e.g., de Vries, 1963; Johansen, 1975; Balland and Arp, 2005). GEOTop uses the one proposed by Cosenza et al. (2003), which was derived in

**Simulating energy and water balance with freezing and terrain effects**

S. Endrizzi et al.

Title Page

Abstract

Introduction

Conclusions

References

Tables

Figures

⏪

⏩

◀

▶

Back

Close

Full Screen / Esc

Printer-friendly Version

Interactive Discussion



analogy to the dielectric permittivity, namely:

$$\lambda_T = \left[ \theta_{sp} \sqrt{\lambda_{sp}} + \theta_w \sqrt{\lambda_w} + \theta_i \sqrt{\lambda_i} + \theta_a \sqrt{\lambda_a} \right]^2 \quad (5)$$

where  $\theta_{sp}$  (–) is the soil porosity, and  $\theta_a$  (–) is the fraction of air or gaseous components, given by

$$\theta_a = \theta_{sp} - \theta_w - \theta_i \quad (6)$$

Equation (2) is integrated assigning the heat fluxes at the upper and lower boundaries of the domain. The upper boundary is given by the interface with the atmosphere or snowpack. At the lower boundary an energy flux is prescribed. This can be assigned externally as a parameter and, depending on the conditions and depth of the soil column, this depends on terrain geometry and transient effects that often overprint the deep geothermal heat flow locally (Gruber et al., 2004). The sink term  $S_{en}$  can also be assigned externally.

### 2.1.1 Soil freezing characteristic curve

Dall’Amico et al. (2011a) derived the soil freezing characteristic curve from the soil water retention curve using the Van Genuchten parameters (Van Genuchten, 1980). They assumed a rigid soil scheme and use the “freezing = drying” assumption (Miller, 1965), which implies that: (i) the freezing (thawing) water is like evaporating (condensing) water; (ii) the ice pressure is equal to the air pressure; (iii) the water and ice content in the soil are related to the soil water retention curve. However, the assumption that ice is always at the air pressure may be restrictive in permafrost modelling, since ice pressure at depth may be significantly high. Nevertheless, this can be extended. Instead of assuming that ice is at the air pressure, it can be more generally supposed that liquid water is not subjected to external pressures, which, on the other hand, are completely supported by the soil matrix and the ice. This entails

## Simulating energy and water balance with freezing and terrain effects

S. Endrizzi et al.

Title Page

Abstract

Introduction

Conclusions

References

Tables

Figures



Back

Close

Full Screen / Esc

Printer-friendly Version

Interactive Discussion



## Simulating energy and water balance with freezing and terrain effects

S. Endrizzi et al.

Title Page

Abstract

Introduction

Conclusions

References

Tables

Figures

⏪

⏩

◀

▶

Back

Close

Full Screen / Esc

Printer-friendly Version

Interactive Discussion



that, when pore water is subjected to an external pressure (e.g., hydrostatic) it starts to freeze, the liquid water is completely unloaded of this pressure once the first ice is formed. Therefore, liquid water pressure would unrealistically undergo a pressure jump when freezing starts. However, since the focus of GEOTop is to simulate soil temperature and moisture dynamics (and not ice pressure), this is deemed reasonable.

## 2.2 Water flow equation

As explained in Appendix B, the system of equations representing the water balance in the soil is:

$$\begin{cases} \frac{\partial \theta_w^{\text{ph}}}{\partial t} + \frac{\rho_i}{\rho_w} \frac{\partial \theta_i}{\partial t} = 0 \\ \frac{\partial \theta_w^{\text{fl}}}{\partial t} + \nabla \bullet \mathbf{J}_w + S_w = 0 \end{cases} \quad (7)$$

where  $d\theta_w^{\text{ph}}$  (–) is the fraction of liquid water content in soil subject to phase change,  $d\theta_w^{\text{fl}}$  (–) is the fraction of liquid water content transferred by water flux,  $\rho_i$  the density of ice ( $\text{kgm}^{-3}$ ),  $\theta_i$  (–) is the fraction of ice in soil, and  $\mathbf{J}_w$  ( $\text{ms}^{-1}$ ) the flux of water in a multiphase mixture. This equation describes the water flow occurring below the soil surface (subsurface flow) and is normally referred to as variably saturated Richards' equation. According to Darcy's law,  $\mathbf{J}_w$  can be written as:

$$\mathbf{J}_w = -K \nabla (\psi + z_f) \quad (8)$$

where  $K$  ( $\text{ms}^{-1}$ ) is the hydraulic conductivity,  $\psi$  (m) the liquid water pressure head and  $z_f$  (m) the elevation head, i.e. the elevation above a reference level. The pressure head in variably saturated conditions is given by (Dall'Amico et al., 2011a):

$$\psi = \begin{cases} \min(0, \psi_{w0}) + \psi_T(T) & \text{if } T < T^* \\ \psi_{w0} & \text{if } T \geq T^* \end{cases} \quad (9)$$

## Simulating energy and water balance with freezing and terrain effects

S. Endrizzi et al.

Title Page

Abstract

Introduction

Conclusions

References

Tables

Figures

⏪

⏩

◀

▶

Back

Close

Full Screen / Esc

Printer-friendly Version

Interactive Discussion

where  $\psi_T(T)$  is the soil matric potential determining the contribute of freezing below the melting temperature  $T^*$  (°C), and  $\psi_{w0}$  (m) is the matric potential corresponding to the total water content. It is assumed that when soil is freezing, the external pressure is completely carried by the ice.

- 5 The water content  $\theta_w$  is calculated by means of the soil water retention curve according to the Van Genuchten (1980) model:

$$\theta_w = \theta_r + (\theta_{sp} - \theta_r) \cdot \{1 + [-\alpha \psi]^n\}^{-m} \quad (10)$$

where  $\theta_r$  (–) is the residual water content and  $\alpha$  (m<sup>-1</sup>), and  $n$  (–) and  $m$  (–) are empirical parameters. Defining  $H$  (m) as the sum of the pressure and potential heads:

$$10 \quad H := \psi + z_f \quad (11)$$

the second part of Eq. (7), combined with Eq. (8), becomes:

$$\frac{\partial \theta_w^{fl}}{\partial t} + \nabla \bullet [-K \nabla H] + S_w = 0 \quad (12)$$

- 15 Since temperature and ice content are kept constant (given by the resolution of the energy balance equation in time lagged manner), the matric potential  $\psi$  is just function of  $\psi_{w0}$ , which is eventually the only unknown of Eq. (12).

- Analogous to the case of water content controlled only by drying processes, the hydraulic conductivity  $K$  is dependent on the soil matric potential  $\psi$  associated with liquid water (Mualem, 1976). However, the presence of ice may significantly reduce the hydraulic conductivity due to the apparent pore blockage effect exerted by ice: this is accounted for by further reducing the hydraulic conductivity by an impedance factor smaller than 1 and equal to  $10^{-\omega q}$  (Hansson et al., 2004; Kurylyk and Watanabe, 2013), where  $\omega$  is a coefficient and  $q$  is the ice fractional content given by  $\theta_i/(\theta_s - \theta_r)$ .

Equation (12) is solved in a fully three-dimensional way in order to describe the both gradients of  $H$  in the direction parallel and normal to the surface. Once the soil

becomes saturated as a result of a precipitation or melting snow, normal gradients may become very small in comparison to those in the parallel direction, which, in turn, are responsible for the routing of water through the soil.

### 2.3 Overland flow

5 The surface (or overland) water flow must also be considered to consistently describe the water balance in the soil and the runoff mechanisms. This process is described with the two-dimensional diffusion wave approximation of the shallow water equation proposed by Gottardi and Venutelli (1993):

$$\frac{\partial \psi|_{z=0}}{\partial t} = \nabla \cdot [\psi|_{z=0} k_s \nabla (\psi|_{z=0} + z_f|_{z=0})] + P_e \quad (13)$$

10 where  $\psi|_{z=0}$  and  $z_f|_{z=0}$  are respectively the liquid water pressure head and the elevation head at the soil surface,  $k_s$  ( $\text{ms}^{-1}$ ) the conductance,  $P_e$  ( $\text{ms}^{-1}$ ) the effective precipitation per unit horizontal surface that reaches the soil surface, including snowmelt flow. The variable  $\psi|_{z=0}$  cannot be negative in this equation and is written in place of the water depth above the surface. Following Gottardi and Venutelli (1993)  
 15 the conductance is

$$k_s = c_s \psi|_{z=0}^\gamma \left( \frac{\partial \psi|_{z=0}}{\partial s} \right)^{-0.5} \quad (14)$$

where  $s$  (m) is the length along the direction of maximum local slope,  $c_s$  the surface roughness coefficient ( $\text{m}^{1-\gamma} \text{s}^{-1}$ ) and  $\gamma$  an exponent between 0 and 1 that varies according to the formulation of  $c_s$ . For example, in the formulation of Manning's it is  
 20  $c_s = n_r^{-1}$  and  $\gamma = \frac{2}{3}$ , where  $n_r$  is Manning coefficient. In the formulation of Chezy it is  $c_s = C_r$  and  $\gamma = \frac{1}{2}$ , where  $C_r$  is the Chezy coefficient. Equation (13) actually works as a boundary condition at the soil surface for Eq. (12).

**Simulating energy and water balance with freezing and terrain effects**

S. Endrizzi et al.

Title Page	
Abstract	Introduction
Conclusions	References
Tables	Figures
⏪	⏩
◀	▶
Back	Close
Full Screen / Esc	
Printer-friendly Version	
Interactive Discussion	



## 2.4 Numerics

In order to reduce the complexity of the numerical method, Eqs. (2) and (12) are linked in a time-lagged manner, instead of solving them in a fully coupled way. Both equations have the same form, which can be generalised as

$$\frac{\partial F(\chi)}{\partial t} + \nabla \bullet [-\kappa(\chi) \nabla \chi] + S = 0 \quad (15)$$

where  $\chi$  is the unknown, function of space and time,  $F$  a non-linear function of the unknown (corresponding to the internal energy content for the heat equation and the total water content for the water flow equation),  $S$  the sink term and  $\kappa$  a conductivity, function of the unknown.

All the derivatives are discretized as finite differences. Therefore, the following relation is obtained:

$$\frac{F(\chi_i^{n+1}) - F(\chi_i^n)}{\Delta t} - \sum_j^M \frac{\kappa_{ij}^m}{D_{ij}} (\chi_j^m - \chi_i^m) + S_i = G_i$$
$$i = 1, 2, \dots, N \quad (16)$$

where the equation is written for the generic  $i$ -th cell,  $n$  represents the previous time step, at which the solution is known,  $n + 1$  is the next time step, at which the solution is unknown.  $\Delta t$  is the time step,  $j$  is the index of the  $M$  adjacent cells with which the  $i$ -th cell can exchange fluxes,  $m$  represents a time instant between  $n$  and  $n + 1$ ,  $\kappa_{ij}$  the conductivity between the cell  $i$  and  $j$ ,  $D_{ij}$  the distance between the centers of the cells  $i$  and  $j$ ,  $S_i$  the sink terms, and  $G_i$  the residual that is to be minimised for finding a solution. Equation (16) is a system of  $N$  equations, and the second term of the left hand side is the sum of the fluxes exchanged with the neighbouring cells. The variables at the instant  $m$  are represented with a linear combination between the instant  $n$  and  $n + 1$ . If  $m = n$  the method is fully explicit and unstable, if  $m = n + \frac{1}{2}$  the method has

Title Page

Abstract

Introduction

Conclusions

References

Tables

Figures



Back

Close

Full Screen / Esc

Printer-friendly Version

Interactive Discussion



a second order precision but may might not be always stable, if  $m = n + 1$  the method has a first order precision but is unconditionally stable. Since there are more concerns on stability than precision, the latter is the chosen method.

A solution of Eq. (16) is sought with a special Newton–Raphson method, with the following sequence (Kelley, 2003):

$$\boldsymbol{\chi}^{n+1} = \boldsymbol{\chi}^n + \lambda_T \boldsymbol{d}(\boldsymbol{\chi}^n) \quad (17)$$

where  $\boldsymbol{\chi}$  and  $\boldsymbol{G}$  are the vectors  $\chi_i$  and  $G_i$  that appear in Eq. (16),  $\boldsymbol{d}$  denotes the Newton direction, and  $\lambda_T$  is a scalar smaller than or equal to 1 referred to as path length, found with a line search method like the Armijo rule (Armijo, 1966). The quantity  $\lambda_T \boldsymbol{d}(\boldsymbol{\chi}^n)$  is also referred to as Newton step. The Newton direction is obtained solving the following linear system

$$\mathbf{G}'(\boldsymbol{\chi}^n) \boldsymbol{d} = -\mathbf{G}(\boldsymbol{\chi}^n) \quad (18)$$

where  $\mathbf{G}'(\boldsymbol{\chi})$  denotes the Jacobian matrix  $\mathbf{G}'(\boldsymbol{\chi})_{ij} = \partial G_i(\boldsymbol{\chi}) / (\partial \chi_j)$ .

If Eq. (15) is solved neglecting the lateral gradients, the number of adjacent cells that are actually considered is maximum 2 (i.e the cell below and above). Therefore, the matrix  $\mathbf{G}'(\boldsymbol{\chi}^n)$  is tridiagonal and symmetric, and then invertible with simple direct methods (El-Mikkawy and Karawia, 2006). On the other hand, if Eq. (15) is solved fully three-dimensionally  $M$  can be up to 6, and, therefore,  $\mathbf{G}'(\boldsymbol{\chi}^n)$  is a symmetric and sparse matrix. Its inversion is a more complex problem (Niessner and Reichert, 1983). In this case, the linear system in Eq. (18) is solved approximatively with an iterative method, the BiCGSTAB Krylov linear solver (Van Der Vorst, 1992). This iterative process becomes an inner iteration, nested in the outer iteration defined in Eq. (17).

### 3 Energy exchange with the atmosphere

The heat flux exchanged with the atmosphere (hereafter referred to as “surface heat flux”) is given by the sum of net shortwave (solar) radiation (SW), net longwave radiation

## Simulating energy and water balance with freezing and terrain effects

S. Endrizzi et al.

Title Page

Abstract

Introduction

Conclusions

References

Tables

Figures

⏪

⏩

◀

▶

Back

Close

Full Screen / Esc

Printer-friendly Version

Interactive Discussion



(LW), and turbulent fluxes of sensible ( $H$ ) and latent heat (LE), namely

$$S(T) = SW + LW(T) + H(T) + LE(T, \theta_w) \quad (19)$$

The surface heat flux is dependent on the temperature of the surface, which is, in turn, the unknown of the equation. In addition, the latent heat flux also depends on the soil moisture at the surface, which is a further coupling term to the water flow equation. All the fluxes in Eq. (19) are positive if they are directed towards the surface. The following section discusses how the components of the surface heat flux are calculated in the simple case of horizontal flat terrain.

### 3.1 Shortwave radiation

The net shortwave radiation appearing in Eq. (19) is a balance given by the incoming radiation  $SW_{in}$  from the atmosphere and the reflected radiation  $SW_{out}$ , which is given by  $SW_{in}$  multiplied by the broadband albedo.

Incoming shortwave radiation on a flat ground surface is the result of the top-of-atmosphere ( $SW_{toa}$ ) shortwave radiation, and atmosphere and cloud transmissivities (respectively  $\tau_a$  and  $\tau_c$ ):

$$SW_{in} = SW_{toa} \tau_a \tau_c \quad (20)$$

While  $SW_{toa}$  can easily be expressed with analytical formulae depending on solar height and azimuth (e.g., Iqbal, 1983), the transmissivities are more complex and uncertain to calculate. The atmosphere transmissivity is here defined as the ratio of the clear-sky incoming shortwave on a flat surface to  $SW_{toa}$ , and is calculated following Meyers and Dale (1983):

$$\tau_a = \tau_R \tau_g \tau_w \tau_{aer} \quad (21)$$

where  $\tau_R$  is the transmission coefficient after Rayleigh scattering,  $\tau_g$  after absorption by permanent gases,  $\tau_w$  after absorption by water vapour, and  $\tau_{aer}$  after absorption and

## Simulating energy and water balance with freezing and terrain effects

S. Endrizzi et al.

Title Page

Abstract

Introduction

Conclusions

References

Tables

Figures



Back

Close

Full Screen / Esc

Printer-friendly Version

Interactive Discussion



scattering by aerosols. These coefficients are expressed as follows, respectively from Atwater and Brown (1974), McDonald (1960), and Houghton (1954):

$$\tau_R \tau_g = 1.021 - 0.084 \left[ m_o \left( 9.49 \times 10^{-4} \cdot p + 0.051 \right) \right]^{0.5} \quad (22)$$

$$\tau_w = 1 - 0.077(w m_o)^{0.3} \quad (23)$$

$$\tau_{aer} = 0.95^{m_o} \quad (24)$$

where  $p$  is the air pressure (in bar),  $m_o$  is the optical air mass (the length of the path through the atmosphere to sea level traversed by light rays), and  $w$  is the precipitable water (in cm) at sea-level pressure (total amount of water vapour in the zenith direction from the sea level to the top of the atmosphere).

The cloud transmissivity is defined as the ratio of the variably cloudy-sky to the clear-sky incoming shortwave on a flat surface, and is a complex function of cloud cover fraction, heights, and types. In GEOTop, this variable is calculated a posteriori from the available measurements of incoming shortwave radiation and also used as a measure of cloud cover in the calculation of incoming longwave radiation, which is not frequently available from measurements. In the few cases when measurements of incoming shortwave radiation are not available and a visual estimation of the cloud cover fraction is available, the cloud transmissivity is obtained from the simple formulation of Kimball (1928), namely

$$\tau_c = 1 - 0.71 \cdot c \quad (25)$$

where  $c$  is the cloud cover fraction, from 0 (clear sky) to 1 (overcast sky).

Albedo is treated differently according to whether the ground surface is snow free or snow covered. In the former case the albedo varies linearly with the liquid water contents of the top soil layer, while, in the latter, the formulation of Dickinson et al. (1993) is used. This formulation (i) accounts for the decrease of the snow reflectance with the time from the last significant snowfall, (ii) partitions the spectrum into visible

## Simulating energy and water balance with freezing and terrain effects

S. Endrizzi et al.

Title Page

Abstract

Introduction

Conclusions

References

Tables

Figures



Back

Close

Full Screen / Esc

Printer-friendly Version

Interactive Discussion





on the cloud-covered fraction of the sky (Deardorff, 1978), which is mostly obtained with visual observation. As an alternative, Crawford and Duchon (1998) proposed a direct relation between the shortwave radiation cloud transmissivity ( $\tau_c$ ) and  $\epsilon_c$ :

$$\epsilon_c = \tau_c + (1 - \tau_c) \cdot \epsilon_a \quad (27)$$

5 which provides a linear interpolation between the clear sky emissivity value and the black-body emissivity in the ideal case of cloud cover completely obscuring the ground. This relation is used in GEOTop since it provides a direct estimation of  $\epsilon_c$  from incoming shortwave radiation without using the cloud-cover fraction of the sky. However,  $\tau_c$  is primarily affected by the cloud cover around the solar disk and not much by cloud  
10 cover far from it. Sicart et al. (2006) showed that this bias is eased if relative long time averages (such as daily) of  $\tau_c$  are taken. In GEOTop this average time is set as a parameter, but normally ranges between 4 h and 1 day. Longer average intervals reduce the cloudiness directionality bias, while shorter ones allow an estimation of the day evolution of the cloud cover. This feature is particularly useful for the estimation  
15 of  $\tau_c$  during the night, which is estimated with a linear interpolation between the value before sunset and after sunrise (Gubler et al., 2012).

The outgoing longwave radiation ( $LW_{out}$ ) emitted by the surface can also be calculated with the Stefan–Boltzmann law:

$$LW_{out} = \epsilon_s \cdot T_{sur,K}^4 \quad (28)$$

20 where  $T_{sur,K}$  is the temperature of the surface (K) and  $\epsilon_s$  is the emissivity of the surface. The latter is set as a parameter if the surface is snow covered. Otherwise, similarly to albedo, it is interpolated between a dry and wet value according to the water content of the first soil layer (Snyder et al., 1998).

## Simulating energy and water balance with freezing and terrain effects

S. Endrizzi et al.

Title Page

Abstract

Introduction

Conclusions

References

Tables

Figures

⏪

⏩

◀

▶

Back

Close

Full Screen / Esc

Printer-friendly Version

Interactive Discussion

### 3.3 Turbulent fluxes

The turbulent fluxes of sensible ( $H$ ) and latent heat (LE) are calculated with the flux-gradient relationship (Brutsaert, 1975b; Panoksky and Dutton, 1984; Garratt, 1992):

$$H = \rho_a c_p w_s \frac{T_a - T_{\text{sur}}}{r_a} \quad (29)$$

$$5 \text{ LE} = \beta_\gamma L_e \rho_a c_p w_s \frac{Q_a - \alpha_\gamma Q_{\text{sur}}^*}{r_a} \quad (30)$$

where  $\rho_a$  is the air density ( $\text{kg m}^{-3}$ ),  $c_p$  the specific heat at constant pressure ( $\text{J kg}^{-1} \text{K}^{-1}$ ),  $w_s$  the wind speed ( $\text{m s}^{-1}$ ),  $T_{\text{sur}}$  the temperature of the surface ( $^\circ\text{C}$ ),  $L_e$  the specific heat of vaporization ( $\text{J kg}^{-1}$ ),  $Q_{\text{sur}}^*$  the saturated specific humidity ( $\text{kg kg}^{-1}$ ) at the surface,  $Q_a$  the specific humidity of the air, and  $r_a$  the aerodynamic resistance  
10 (–). The  $\alpha_\gamma$  and  $\beta_\gamma$  coefficients take into account the soil resistance to evaporation, and only depend on the liquid water pressure close to the the soil surface. They are calculated according to the parameterization of Ye and Pielke (1993), which considers evaporation as the sum of the proper evaporation from the surface and diffusion of  
15 water vapour in soil pores at greater depths. The aerodynamical resistance is obtained applying the theory of Monin Obukhov (Monin and Obukhov, 1954), which requires that known values of wind speed, air temperature, and specific humidity are available at least at a two different heights above the surface. Known values at only one height above the surface are sufficient if it is assumed that just above the surface (properly at  
20 zero height above the surface): (i) the value of air temperature is equal to the value of soil temperature at the surface (this assumption also leads to the boundary condition non-linearity), (ii) the specific humidity is equal to  $\alpha_\gamma Q_{\text{sur}}^*$ , and (iii) wind speed is zero.

## 4 Complex terrain

Complex terrain significantly complicates the representation of the surface heat flux with respect to the ideal flat terrain case. In this paragraph it is shown how the effects of complex terrain are accounted for the components of the surface heat flux.

### 4.1 Shortwave radiation

Incoming shortwave radiation is always partitioned in two components: a direct component that comes from the direction of the sun, and a diffuse component assumed to be isotropic (see also Formetta et al., 2013). Since incoming shortwave radiation is often measured as global (i.e. sum of direct and diffuse components), it becomes important to differentiate in its direct and diffuse portions since the two components react differently to complex terrain. Erbs et al. (1982) provided an empirical expression relating  $k_t$ , the ratio of the hourly diffuse radiation to the hourly global radiation, to the ratio of the hourly global radiation to the hourly radiation at the top of the atmosphere (namely  $\tau_a \cdot \tau_c$ ). So far all the radiation components are relative to flat surfaces.

In complex terrain: (i) the direct component is obtained multiplying the direct component for the flat surface by the ratio  $\frac{\cos(\theta_n)}{\cos(\theta_v)}$ , where  $\theta_n$  is the angle between the normal to the surface and the direction of the sun, and  $\theta_v$  the angle between the vertical and the direction of the sun (solar angle deviation); (ii) the direct component may be shaded by the surrounding topography (cast shadow) or it can happen that the angle  $\theta_n$  be larger than  $90^\circ$  (self shadow); (iii) there is also a component of incoming shortwave resulting from reflections from the surrounding terrain, which are assumed to be isotropic in the terrain view angle; and (iv) the diffuse radiation coming from the sky, assumed isotropic, has to be reduced according to the visible sky angle.

The incoming shortwave radiation is calculated as follows:

- Clear-sky global radiation on a flat terrain surface is obtained from Eq. (20).

## GMDD

6, 6279–6341, 2013

### Simulating energy and water balance with freezing and terrain effects

S. Endrizzi et al.

Title Page

Abstract

Introduction

Conclusions

References

Tables

Figures

⏪

⏩

◀

▶

Back

Close

Full Screen / Esc

Printer-friendly Version

Interactive Discussion

## Simulating energy and water balance with freezing and terrain effects

S. Endrizzi et al.

Title Page

Abstract

Introduction

Conclusions

References

Tables

Figures



Back

Close

Full Screen / Esc

Printer-friendly Version

Interactive Discussion

- Cloud transmittance is obtained either from Eq. (25) or as the ratio of measured global radiation to clear-sky global radiation (both on a flat terrain surface).
- The diffuse and direct portions of incoming shortwave radiation on a flat ground surface are calculated according to the formula of Erbs et al. (1982). The diffuse radiation obtained is referred to as hemispheric diffuse radiation, because it considers the sky unobstructed.
- Direct radiation is corrected according to topography, accounting for shadowing and solar incidence angle.
- Diffuse radiation is calculated as two components: (i) one coming from the atmosphere calculated multiplying the hemispheric diffuse radiation by the sky view factor ( $V_f$ ), which is a topographical parameter that accounts for the portion of the sky that is actually seen from a pixel and varies from 0 (sky not visible) to 1 (flat terrain case, where the sky view angle is the entire hemisphere); and (ii) a second component resulting from the shortwave radiation reflected from the terrain seen from the pixel (surrounding terrain). This component can be calculated with complex algorithms that account for all pixels visible from the pixel of interest  $p$  (Helbig et al., 2009). This is not performed in GEOTop, which, instead, calculates this radiation component with either of two simple methods: either it is considered that the terrain surrounding a generic pixel  $p$  has the same outgoing shortwave radiation as  $p$  (that is  $SW_{out,p}$ ), and, so, the radiation from the surrounding terrain is given by  $(1 - V_f) \cdot SW_{out,p}$  (one-dimensional approximation), or the average of outgoing shortwave radiation in a certain area is taken ( $SW_{out,av}$ ) and the radiation from the surrounding terrain is considered as  $(1 - V_f) \cdot SW_{out,av}$  (two-dimensional approximation).

## 4.2 Longwave radiation

As for diffuse shortwave radiation, in complex terrain incoming longwave radiation comes from both the atmosphere and the surrounding terrain. The former is given by the incoming longwave radiation calculated as in the flat case multiplied by  $V_f$ .

5 The component emitted from the surrounding terrain is calculated with the same two methods shown for shortwave radiation.

## 4.3 Turbulent fluxes

The turbulent exchange in complex terrain has been observed to significantly deviate from the theory of Monin–Obukhov, which is built from the premise that terrain is flat and infinitely homogeneous (e.g., De la Casiniere, 1974). In particular, a maximum wind speed is often observed near the surface as a result of wind gravity flows, whereas according to the theory the wind profile should be logarithm (in neutral atmosphere) with a small deviation due to temperature gradients (Halberstam and Schieldge, 1981; Meesters et al., 1997; Wagon et al., 1999). Including these effects in a model like  
15 GEOTop would require solving the Navier–Stokes equations for the wind field, which is beyond the purposes of the model. However, it has been also observed (e.g., Denby and Greuell, 2000) that if the measurements of wind, temperature and relative humidity are performed as close as possible to the surface, the conditions are actually closer to the assumptions of the theory of Monin–Obukhov, and, therefore, the results are  
20 supposed to be more accurate.

Since meteorological variables are measured only at a limited number of locations, a measurement distribution method is required to assign meteorological forcings (wind, temperature, and relative humidity) for the surface energy balance to the whole surface. This issue is described in Appendix D.

## Simulating energy and water balance with freezing and terrain effects

S. Endrizzi et al.

Title Page

Abstract

Introduction

Conclusions

References

Tables

Figures

⏪

⏩

◀

▶

Back

Close

Full Screen / Esc

Printer-friendly Version

Interactive Discussion



## 5 Snow cover

The snow cover plays an important role as it buffers the energy and mass exchanges between the atmosphere and soil. Important processes related to the snow cover dynamics include snow warming and cooling, melting and refreezing, water percolation, accumulation due to snow precipitation, avalanches, deposition of wind blown snow, erosion due to wind, and densification due to snow metamorphism.

The system of equations for snow is similar to the set of Eqs. (1) and (7) used for the soil matrix, as snow may also be considered a porous material. However, snow has the following peculiarities: (a) the snow volume of control is ephemeral, i.e. it may disappear as a result of melting; (b) the rigidity to the structure is given by the ice grains; (c) the porosity of snow  $\phi_s$  is variable and depends on the ice content  $\theta_{is}$ ; (d) the control volume is not fixed, but is subject to variations due to accumulation, compaction and melting processes; (e) the capillarity effects are in general not significant (Jordan, 1991).

In GEOTop snow is computed solving in sequence: (i) the heat equation, (ii) snow metamorphism, (iii) water percolation, (iv) accumulation. The simplified effects of avalanches and blowing snow are also considered, but they will not be dealt with in this paper.

### 5.1 Snow volumetric system

Let us call  $V_s$  the control volume ( $m^3$ ) of snow: the sum of the liquid, solid and gaseous contents in the volume must equal 1 for continuity:

$$\theta_{ws} + \theta_{is} + \theta_g = 1 \quad (31)$$

where  $\theta_{ws}$  (–) is the liquid volumetric fraction,  $\theta_{is}$  (–) the solid water volumetric fraction, and  $\theta_g$  (–) the gaseous volumetric fraction. Considering that the rigidity to the structure is given by the ice grains, snow porosity  $\phi$  (–) may be calculated as the available pores

## Simulating energy and water balance with freezing and terrain effects

S. Endrizzi et al.

Title Page

Abstract

Introduction

Conclusions

References

Tables

Figures

⏪

⏩

◀

▶

Back

Close

Full Screen / Esc

Printer-friendly Version

Interactive Discussion



excluding the ice grains, i.e.:

$$\phi_s = \theta_{ws} + \theta_g = 1 - \theta_{is} \quad (32)$$

Snow porosity is not constant as it depends on the snow metamorphism.

## 5.2 Heat equation

5 Following the approach used for the soil, the heat equation for snow becomes similar to Eq. (B7), the internal energy of the snow being:

$$U_s = (\rho_i c_i \theta_{is} + \rho_w c_w \theta_{ws})(T_s - T_{ref}) + L_f \rho_w \theta_{ws} \quad (33)$$

10 where  $T_s$  (°C) is the snow temperature. The heat equation is solved neglecting the lateral gradients with the same numerical method used to solve the heat equation in the soil. The boundary condition at the interface with the atmosphere is given by the surface heat flux, as described in the previous section. At the interface with the soil surface the heat exchange is given by the conduction heat flux, which is dependent on the temperature gradient in proximity to the interface. This last exchange flux actually couples the heat equations in the soil and snow, which have to be solved together in a system.

15 A freezing characteristic curve is defined also for snow in order to derive an expression for the apparent heat capacity. However, the phase change in the snow takes place virtually at 0°C, since the pores are large enough that temperature depressions due to capillarity effects are not significant (Jordan, 1991). The definition of a freezing characteristic curve has mostly a numerical reason, therefore the curve must approach as much as possible a step function in correspondence of 0°C. A simple relation relating temperature and the ratio between liquid water content and total water content in the snow is used (Jordan, 1991):

$$\frac{\theta_{ws}}{\theta_{ws} + \frac{\rho_i}{\rho_w} \theta_{is}} = \frac{1}{1 + (a T_s)^2} \quad (34)$$

where  $a$  ( $^{\circ}\text{C}^{-1}$ ) is a constant. The higher value this constant is set to, the closer to a step function the curve is, but, at the same time, the more difficult the numerical resolution is. Jordan et al. (1999) set the constant to  $10^2$ . However, values up to  $10^5$  can be assigned.

The heat flux at the soil–snow interface is calculated defining an effective thermal conductivity at the interface, and the temperature gradient calculated with the temperatures of the lowest snow layer and the top soil layer. The effective thermal conductivity is sought in a similar way as the effective thermal conductivities at the interfaces between soil layers. Formulae, like Eq. (5) proposed by Cosenza et al. (2003) provide a relation of the overall conductivity to the conductivities and volumetric ratios of the single constituents. The effective thermal conductivity is obtained linearly interpolating the volumetric contents of liquid water, ice, air, and soil matrix at the interface.

The thermal conductivity of snow can be calculated also with the formula of Cosenza et al. (2003), or with other formulations (Sturm et al., 1997; Yen, 1981; Calonne et al., 2011).

### 5.3 Metamorphism

GEOtop describes the densification that the newly fallen snow rapidly undergoes (destructive metamorphism) as well as the slow compaction process as a result of the snow weight (overburden), using the empirical formulae of Anderson (1976), improved by Jordan (1991) and Jordan et al. (1999). The constructive metamorphism leading to new shapes of the snow crystals, like hoar layers, is not represented.

The equation describing snow densification is applied separately for each snow layer and is written as (Anderson, 1976):

$$\frac{1}{D} \frac{\partial D}{\partial t} = C_1 + C_2 \quad (35)$$

## GMDD

6, 6279–6341, 2013

### Simulating energy and water balance with freezing and terrain effects

S. Endrizzi et al.

Title Page

Abstract

Introduction

Conclusions

References

Tables

Figures

⏪

⏩

◀

▶

Back

Close

Full Screen / Esc

Printer-friendly Version

Interactive Discussion



## Simulating energy and water balance with freezing and terrain effects

S. Endrizzi et al.

Title Page

Abstract

Introduction

Conclusions

References

Tables

Figures

⏪

⏩

◀

▶

Back

Close

Full Screen / Esc

Printer-friendly Version

Interactive Discussion



where  $D$  is the thickness of the snow layer, and  $C_1$  and  $C_2$  are respectively the total fractional compaction rate ( $\text{s}^{-1}$ ) as a result of destructive metamorphism and overburden. Equation (35) is integrated with the same time step  $\Delta t$  used for the heat equation, assuming that the snow layer has a thickness  $D_0$  (known) at the beginning of the time step and a thickness  $D_1$  at the end. The integration is carried out as follows:

$$\int_{D_0}^{D_1} \frac{dD}{D} = \int_0^{\Delta t} (C_1 + C_2) dt \quad (36)$$

which gives

$$D_1 = D_0 \exp(C_1 + C_2) \Delta t \quad (37)$$

The total fractional compaction rates are given by Anderson (1976) eventually modified by Jordan et al. (1999):

$$C_1 = -\alpha_s \exp(-0.04 \cdot T_s) \quad (38)$$

where  $\alpha_s$  equals to:

$$\begin{cases} \alpha_s = -2.778 \times 10^6 \cdot c_3 \cdot c_4 \\ \text{if } \rho_1 \theta_{is} \leq 100: c_3 = 1 \\ \text{if } \rho_1 \theta_{is} > 100: c_3 = \exp[-0.046(\rho_1 \theta_{is} - 100)] \\ \text{if } \rho_w \theta_{ws} = 0: c_4 = 1 \\ \text{if } \rho_w \theta_{ws} > 0: c_4 = 2 \end{cases} \quad (39)$$

The above equation states that a compaction of  $1\% \text{h}^{-1}$  (Anderson, 1976) is present at a snow density smaller than or equal to  $100 \text{kgm}^{-3}$  (cutoff density) at  $0^\circ\text{C}$  and without liquid water. If liquid water is present, the coefficient is increased by 50%.

For densities larger than the cutoff density,  $\alpha_s$  decreases very rapidly, becoming one tenth at a density of  $150 \text{ kg m}^{-3}$  and one hundredth at  $200 \text{ kg m}^{-3}$ . Furthermore, the compaction increases with snow temperature, and doubles at a temperature of about  $-17^\circ\text{C}$ .

5 The parameter  $C_2$  is related to the ratio between the weight of the overlying snow column  $P_s$  ( $\text{N m}^{-2}$ ) calculated at the centre of the considered snow layer and the snow viscosity  $\eta$  ( $\text{N s m}^{-2}$ ):

$$C_2 = -\frac{P_s}{\eta} \quad (40)$$

where

$$10 \quad \eta = 3.6 \times 10^6 \exp(-0.08 \cdot T_s) \cdot \exp(0.021 \cdot \rho_{\text{sn}}) \quad (41)$$

being  $\rho_{\text{sn}} := \rho_i \theta_{\text{is}} + \rho_w \theta_{\text{ws}}$  ( $\text{kg m}^{-3}$ ) the snow density.

Densification takes place also when melting occurs. When ice melts in a specific snow layer, it is considered that the thickness of the layer reduces proportionally to the ice content. This makes sense, as the snow depth is a result of the ice grains structure.

15 This leads to an increase in density, since the same total water content will occupy a smaller volume. Densification occurs also when liquid water starts to refreeze and the new ice will fill the empty pores. On the other hand, a snow layer may be subject to a density decrease as a result of the percolation process, because the total water volume in the layer will decrease, but not its volume.

20 Another snow densification process is related to wind loads. When the wind speed is higher than a threshold (set to the wind value at which snow starts to be drifted), the wind load is considered as an additional overburden. This describes the snow packing at the surface, which leads to a progressive resistance to being drifted (Liston and Elder, 2006b).

## Simulating energy and water balance with freezing and terrain effects

S. Endrizzi et al.

Title Page

Abstract

Introduction

Conclusions

References

Tables

Figures

⏪

⏩

◀

▶

Back

Close

Full Screen / Esc

Printer-friendly Version

Interactive Discussion



## 5.4 Water percolation

The equation governing the water balance in each snow layer is the second part of Eq. (7), which, considering a 1-D discretisation and integrating along the vertical direction, results in:

$$5 \quad \frac{\partial \theta_{ws}^{fl}}{\partial t} + \frac{J_{ws}^{up} - J_{ws}^{dw}}{D} + S_{ws} = 0 \quad (42)$$

where  $J_{ws}^{up}$  ( $\text{ms}^{-1}$ ) is the incoming flux from above and  $J_{ws}^{dw}$  is the outgoing downward flux. Following Colbeck (1972), the flux  $J_{ws}$  occurs as soon as  $\theta_{ws}$  reaches a certain threshold value accounting for the capillary retention, i.e. the irreducible water saturation  $S_r$  (-), which is set as a snow porosity fraction ( $S_r \cdot \phi_s$ ).  $S_r$  normally ranges  
10 between 4 and 7% (Colbeck, 1972). The flux  $J_{ws}$  is calculated according to Darcy's law but neglecting the capillarity effects and using only the gravimetric gradient:

$$10 \quad \begin{cases} \text{if } \theta_{ws} \geq S_r \cdot \phi_s: J_{ws} = -K_s \cos \beta \\ \text{else } J_{ws} = 0 \end{cases} \quad (43)$$

where  $\beta$  ( $^\circ$ ) is the local slope angle and  $K_s$  ( $\text{ms}^{-1}$ ) is the hydraulic conductivity for snow.  $K_s$  is calculated according to the model of Brooks and Corey (1964), as in Jordan  
15 (1991):

$$K_s = K_{s,max} S_e^3 \quad (44)$$

where  $K_{s,max}$  ( $\text{ms}^{-1}$ ) the maximum hydraulic conductivity for the snow, and  $S_e$  (-) is the effective saturation, which is given by

$$20 \quad S_e = \frac{\theta_{ws} - S_r \cdot \phi_s}{\phi_s - S_r \cdot \phi_s} \quad (45)$$



## Simulating energy and water balance with freezing and terrain effects

S. Endrizzi et al.

Title Page

Abstract

Introduction

Conclusions

References

Tables

Figures

⏪

⏩

◀

▶

Back

Close

Full Screen / Esc

Printer-friendly Version

Interactive Discussion



Fresh snow density depend on grain size and crystal type, as they affect the way fresh snow is deposited. Smaller grains with simpler shape pack more efficiently and lead to denser snow. These effects, however, are indirectly described parameterising the density in function of air temperature and wind, which are easier to measure and have been correlated to fresh snow density in several studies (e.g., McGurk et al., 1988). The following formula proposed by Jordan et al. (1999) is used, which incorporates both temperature and wind effects

$$\rho_{\text{ns}} = \begin{cases} 500 - 475.5 \exp \left[ -1.4(5.0 - T_a)^{-1.15} - 8 \cdot \frac{w_s^{1.7}}{1000} \right] & \text{if } T_a > 13^\circ\text{C} \\ 500 - 452.0 \exp \left[ -8 \cdot \frac{w_s^{1.7}}{1000} \right] & \text{elsewhere} \end{cases}$$

where  $\rho_{\text{ns}}$  is the density of the new snow ( $\text{kg m}^{-3}$ ).

### 5.6 Discretisation

The snowpack, according to the thermal gradients, may be roughly classified into three regions: an upper, middle, and bottom portion. In the upper and bottom regions the vertical gradients are often high, as a result of the interactions with the atmosphere and the underlying soil respectively. On the other hand, in the middle region the vertical gradients are weaker. The snow discretisation in GEOtop is done in order to accurately describe the thermal gradients in the snowpack and avoid the allocation of unnecessary memory. The total number of layers, in fact, depends on the mass of snow present, whereas the distribution of layers in the snowpack privileges the upper and bottom zones.

GEOtop requires four parameters to set the snow layering scheme:

- $M_{\text{up}}^*$  and  $M_{\text{dw}}^*$  ( $\text{kg m}^{-2}$ ), which are the maximum mass per unit area of the snowpack in the upper and bottom regions, respectively;

## Simulating energy and water balance with freezing and terrain effects

S. Endrizzi et al.

Title Page

Abstract

Introduction

Conclusions

References

Tables

Figures

⏪

⏩

◀

▶

Back

Close

Full Screen / Esc

Printer-friendly Version

Interactive Discussion

- $M_l^*$  ( $\text{kg m}^{-2}$ ), which is the maximum admitted mass for a single layer (it must be  $M_l^* \leq M_{\text{up}}^*$  and  $M_l^* \leq M_{\text{dw}}^*$ );
- $N_{\text{mid}}^*$  (–), which is the maximum number of layers admitted in the middle region.

The mass of snow per unit area ( $\text{kg m}^{-2}$ ) present in a layer  $l$  is referred to as  $M_l$ , and the total mass of snow per unit area present in the snowpack is named  $M_{\text{tot}}$ . As described in Table 5, the number of regions used to describe the snowpack depends on  $M_{\text{tot}}$ : (i) if  $M_{\text{tot}} < M_{\text{up}}^*$ , only the upper region is used, which extends throughout the whole snowpack; (ii) if  $M_{\text{tot}}$  is larger than  $M_{\text{up}}^*$ , but smaller than  $M_{\text{up}}^* + M_{\text{dw}}^*$ , also the bottom region is created with mass  $M_{\text{tot}} - M_{\text{up}}^*$ ; (iii) if  $M_{\text{tot}} > M_{\text{up}}^* + M_{\text{dw}}^*$ , then also the middle region is defined.

At each time step the layers are re-organized (in number, thickness, mass content and internal energy) according to the evolution of the snowpack. In particular, as outlined in Table 6, three processes may occur:

- Layer splitting: if the mass of the top snow layer as a result of new snow accumulation exceeds the maximum allowed mass ( $M_l > M_l^*$ ), then it is split in two layers in such a way that the lower new layer keeps a mass equivalent to  $M_l^*$  and the new surface layer has the remainder of the mass. In case the total mass of the upper region exceeds the threshold  $M_{\text{up}}^*$ , then the lower layer of the upper portion is pushed to the middle or lower region.
- Layers merging: two adjacent layers may be merged into one layer that will have the sum of ice and liquid water content of the layers to merge, and temperature resulting from the energy content given by the sum of the energy contents of the layers to merge. Layer merging happens in the following cases: (i) if the number of layers of the middle zone  $N_{\text{mid}}$  exceed  $N_{\text{mid}}^*$ , then two adjacent layers of the middle zone are merged. The choice falls on the two adjacent layers that have the smallest combined mass: this allows keeping the layers in the middle region

of similar snow mass content and prevents from excessively smoothing the snow vertical profile; (ii) if a snow layer completely loses its ice mass in a one-time-step integration of the heat equation, the snow layer that would disappear is merged with the underlying layer and then the heat equation is re-integrated.

## 6 Testing GEOtop

To add credibility to the results of the subsequent experiment, we demonstrate here that GEOtop produces plausible results in its major components. We also discuss the error inherent in linking the heat and water flow equations in a time-lagged manner instead of coupling them is evaluated experimentally. For this, we initialise a 0.3 m deep column of sandy loam with a uniform pressure head of  $-0.1$  m and a linear temperature profile between  $0^{\circ}\text{C}$  at the top and  $-1^{\circ}\text{C}$  at the bottom. No energy and water is exchanged with the outside. Running this simulation over time, the temperature of the soil column will approach a uniform value and pressure gradients due to freezing will redistribute water. Finally, to estimate the magnitude of error inherent in using a linked solution, we compare results based on time steps of 1 s and 1 h. The temperature and total water content (i.e. liquid and frozen) as well as deviations between both simulations are shown in Fig. 1. As the deviations in temperature are negligible and those in liquid water are on the order of  $\pm 6\%$ , the linked solution is deemed acceptable in this context. The performance of the frozen soil model has been evaluated by comparison with analytical solutions and experimental results by Dall'Amico et al. (2011a).

The representation of the snowpack is evaluated by comparison of a simulation with measurements (Morin et al., 2012) at Col de Porte. Similar to the evaluation of the simulator Crocus by Vionnet et al. (2012), we quantify performance based on daily averages of snow depth and water equivalent using the bias and the root mean squared deviation (RMSD) for the months December to May during the years 2001 to 2011. For snow water equivalent, we obtain a RMSD of 37.1 mm (39.7, 37.0 mm) and a bias of  $-3.2$  mm ( $-17.3$ ,  $-2.3$  mm). For snow depth, the RMSD is 0.15 m (0.11,

## Simulating energy and water balance with freezing and terrain effects

S. Endrizzi et al.

Title Page

Abstract

Introduction

Conclusions

References

Tables

Figures



Back

Close

Full Screen / Esc

Printer-friendly Version

Interactive Discussion





lowest 15 layers have thicknesses ranging from 0.2 to 0.5 m whereas the remaining layers have thickness of 0.1 m. Overall, the soil domain reaches a depth of 10.5 m.

Topographical differences have been created by varying the inclination angle of the lateral slopes ( $\beta$  in Fig. 2) from 5 to 20°. The longitudinal slope (from point 3 to 4 in Fig. 2) of 5° and the average elevation (3000 m) are kept constant. The two topographies are hereafter referred to as 5 and 20° topography, respectively.

The following water balance configurations, which are here referred to for simplicity as 3-D, 1-D, and 0-D, are considered. 3-D means that the full three-dimensional variably saturated Richards equation with the surface flow is used. In 1-D, the Richards equation is solved only in one-dimension, i.e. in the vertical, and no lateral subsurface drainage is considered. Surface flow occurs as lateral flow only on the surface. In 0-D, the soil water balance is not solved, and no infiltration is described. Therefore, the total water content always remains at its initial value, however, soil water will undergo freezing and thawing.

Six simulations have been then performed: 5° (topography) 3-D, 5° 1-D, 5° 0-D, 20° 3-D, 20° 1-D, and 20° 0-D. They have been run for the hydrological year 2001–2002 (from 1 October 2001 to 30 September 2002) using meteorological data measured at the station of Davos, Switzerland, located at 1595 m a.s.l. and operated by Meteoswiss. This year was chosen because it is the most similar to the average year in the 1981–2010 period, if the cumulated winter precipitation (from October to May) and the average air temperature in the summer (from June to September) are considered. The first quantity represents a proxy for snow precipitation and the second one approximates summer warming. Respective values are 452 mm and 10.6°C for the hydrological year 2001–2002, and 479 mm and 10.6°C for the average year in the period 1981–2010 period.

The system was initialized considering an absence of snow cover, uniform soil temperature of -1°C, and soil deeper than 1 m saturated, and hydrostatic pressure profile in both the saturated and unsaturated portions (prolonging the hydrostatic pressure profile also for negative pressures). However, in order to reduce the influence

## Simulating energy and water balance with freezing and terrain effects

S. Endrizzi et al.

Title Page

Abstract

Introduction

Conclusions

References

Tables

Figures



Back

Close

Full Screen / Esc

Printer-friendly Version

Interactive Discussion



## Simulating energy and water balance with freezing and terrain effects

S. Endrizzi et al.

Title Page

Abstract

Introduction

Conclusions

References

Tables

Figures

⏪

⏩

◀

▶

Back

Close

Full Screen / Esc

Printer-friendly Version

Interactive Discussion

of the arbitrariness of the initial condition, a spin-up simulation has been performed for 100 yr. At the end of the spin-up the catchment is still completely underlain by permafrost, with active layer depths ranging from 1 to 7 m. Since the response time of permafrost soil is extremely slow, a longer spin-up simulation would probably enhance the spatial variability of the active layer depth and completely thaw permafrost in some part of the catchments. However, a 100 yr spin-up is considered acceptable in this context, since we are mainly interested in the approach evaluation.

In order to evaluate the set of simulations the following steps are followed: (i) annual average variables in the single points shown in Fig. 2 are compared, (ii) annual average distributed variables are compared and their spatial distribution in the catchment discussed, and (iii) the time evolution of some variables for a selected point is shown. Figure 3 shows the mean annual temperature at a 4 m depth, the active layer depth (considered as the lowest depth of thaw reached during the summer), and the annual average water table depth (the average was calculated only when there is actually a water table) for the six points for the six simulations. Point 1 and 2 are both on the south slope at short distance apart and have very similar temperature values, but the different topographies and water balance descriptions give significantly different values of temperatures, which range between  $+0.3^{\circ}\text{C}$  (permafrost thawed) and slightly negative values (permafrost still present at a 4 m depth). The active layer and water table depth show significant differences in the simulations (of the order of 1–2 m), with slightly deeper values for Point 2, which is downstream. Point 3 and 4 are located in the channel portion and also exhibit similar values. The results of the six simulations give temperature ranges between slightly positive and slightly negative values and differences of the order of 1–2 m in active layer and water table depths. Points 5 and 6 are located in the north slope and results significantly colder than the other points, with temperatures ranging from  $-1^{\circ}\text{C}$  and slightly negative values, and active layer and water table depths ranging from 0.3 to 1 m. It is therefore important to notice that both different topographies and different hypotheses on soil water balance have a significant effect on the results.

## Simulating energy and water balance with freezing and terrain effects

S. Endrizzi et al.

Title Page

Abstract

Introduction

Conclusions

References

Tables

Figures

⏪

⏩

◀

▶

Back

Close

Full Screen / Esc

Printer-friendly Version

Interactive Discussion

Figure 4 shows the spatial distribution of the active layer depth and the depth of thaw. If the water balance is not solved (0-D simulation), the spatial variability of the active layer is given by aspect and elevation only. In the north slope the values are rather homogeneous around 1 m, while in the south slope they are significantly dependent on altitude, ranging from 1 m at the top to 3 m at the bottom for the 5° topography, and from 4 to 7 m for the 20° topography. If the water balance is solved 1-D, the effect of altitude and aspect is attenuated, and the spatial variability reduced. If a full 3-D water balance is considered, a clear relation between active layer depth and water table can be recognized. Where water table is shallower and, therefore, soil is wetter, the active layer is deeper. In the 5° topography, the water table at the lowest elevations of the south slope is at the surface. For mid elevations water table depth reaches a maximum value of about 2 m, and then for higher elevations it decreases to values of about 1–1.5 m. This is probably a consequence of the strong dependance of active layer on elevation. However, the active layer depth has a larger spatial variability than in the 0-D water balance case, since it reaches values up to 5 m at the bottom of the south slope (instead of 3 m) and up to 2.5 m at the bottom of the north slope (instead of 1 m). This is probably a result of the interplay between soil moisture and freezing-thawing energetics, which is added to the spatial variability induced by slope and aspect. The 20° topography has similar features, but the lateral drainage in this steeper topography adds active layer spatial variability in a lesser degree than in the 5° topography.

Figure 5 shows the temporal evolution of temperature, and liquid, solid and total water content in soil and snow for point 1 shown in Fig. 2. All charts also report the lower and upper boundaries of the thawed layer, and the water table. Temperature is in general negative and close to 0 °C except at the surface. The soil is completely frozen from mid December to mid June, and the thawed portion reaches the maximum depth in mid September, which is kept until almost mid November, when the freezing front from above, starting in October, gets significantly low. The charts of liquid water, ice and total water content show that three regions, from top to bottom, can roughly be distinguished: (i) a region relatively rich in total water at the top (hereafter referred to as “wet region”),

## Simulating energy and water balance with freezing and terrain effects

S. Endrizzi et al.

Title Page

Abstract

Introduction

Conclusions

References

Tables

Figures

⏪

⏩

◀

▶

Back

Close

Full Screen / Esc

Printer-friendly Version

Interactive Discussion

(ii) a drier region in the lower portion of the active layer (“dry region”), and (iii) the “undisturbed frozen region” below. The wet region starts to develop in the autumn when the active layer starts freezing and is initially bordered below by the freezing front. It gets then wetter as a result of early snow melting and, probably, water transfer from slightly warmer dry region below. Liquid water content is low ( $< 0.1$ ) and ice content is high ( $> 0.3$ ) when the wet region is frozen, and temperature is significantly low (around  $-2^{\circ}\text{C}$ ). When the wet region thaws in the summer it gets even wetter as a result of infiltration. However, thawing takes place at a relatively slow rate in this region, as a result of the high ice content and, therefore, the high energy content required to melt it. The dry region has slowly lost the initial water content in many years due to the lateral drainage during the summer. When the thawing front reaches this region in late summer, the thawed soil depth sharply increases because the energy required to thaw the soil is relatively low. At the same time a large amount of liquid water is drained from the wet region above, which virtually disappears. This amount of liquid water is gradually drained horizontally, and it eventually accumulates in a thin layer in the lower part of the region. This layer gets thinner as the season progresses, but it does not immediately disappear when the region freezes in early winter, as a result of relatively high (though negative) temperature. The undisturbed region below was never affected by summer thawing, and the total water content is still dependent on the initial condition. Even though a spin-up simulation has been performed for 100 yr, it is not guaranteed that an equilibrium state has been reached, and, therefore, a longer spin-up simulation could entail different conditions.

## 8 Conclusions

GEOtop 2.0 presents a novel combination of represented processes and solves a fully three-dimensional form of the Richards and shallow water equations. It uses a simplified, but physically consistent parameterisation of the soil water retention curve to describe soil freezing characteristics in saturated and unsaturated conditions. In

its numerical implementation, GEOTop 2.0 uses sophisticated integration methods, which allow convergence even in cases where parameters have nearly discontinuous behaviour, and results in proper conservation mass and energy. This allows the investigation of complex hydrologic phenomena in cold regions for which no compound parameterization may exist.

In experiments shown, the model showed a consistent physical realism and comparison with snow cover data resulted in reasonable agreement. An experiment with differing model structure, realized by differing treatment of water transport in the soil, highlighted that significant differences of temperature, water fluxes, and water table depths can result from this. Furthermore, the spatial differentiation of these results in response to topography highlights the complex nature of the phenomena investigated and represented.

GEOTop 2.0 represents a wider range of processes in the water and the energy budgets at small scales than most other simulators. It thus allows studying their interactions without introducing “ad hoc” solutions that may compromise the representation of complexity. In this publication, we have described the details and functioning of small-scale hydrology and its interaction with frozen soil and snow cover. Its effect on catchment discharge will be evaluated in the future.

## Appendix A

### Use and license of GEOTop

GEOTop 2.0 is provided with a GNU General Public License, version 3 (GPL-3.0). The source code, a first version of the manual (Dall’Amico et al., 2011b), and some template simulations are available through google code at the address: <https://code.google.com/p/geotop/>. Gubler et al. (2013) provide a good starting point for the selection of many parameter values, however, optimal choices and sensitivities may differ from application to application.

## Simulating energy and water balance with freezing and terrain effects

S. Endrizzi et al.

Title Page

Abstract

Introduction

Conclusions

References

Tables

Figures



Back

Close

Full Screen / Esc

Printer-friendly Version

Interactive Discussion





The components “fl” and “ph” of the internal energy may be derived starting from the definition of the internal energy  $U$  (Dall’Amico et al., 2011a):

$$U = C \cdot (T - T_{\text{ref}}) + L_f \rho_w \theta_w \quad (\text{B7})$$

where  $C := \rho_{\text{sp}} c_{\text{sp}} (1 - \theta_{\text{sp}}) + \rho_i c_i \theta_i + \rho_w c_w \theta_w$  is the volumetric heat capacity ( $\text{J m}^{-3} \text{K}^{-1}$ ).

5 Differentiating Eq. (B7) one obtains:

$$\begin{aligned} dU &= C dT + (T - T_{\text{ref}}) dC + L_f \rho_w d\theta_w \\ &= C dT + \rho_i c_i d\theta_i (T - T_{\text{ref}}) + u_f d\theta_w \end{aligned} \quad (\text{B8})$$

where:

$$10 \quad u_f := \rho_w [L_f + c_w (T - T_{\text{ref}})] \quad (\text{B9})$$

From the first equation in B6 the variation of the ice content may be referred to the variation of  $\theta_w^{\text{ph}}$ :

$$d\theta_i = -\frac{\rho_w}{\rho_i} d\theta_w^{\text{ph}} \quad (\text{B10})$$

Substituting Eqs. (B3) and (B10) in Eq. (B8), after some calculations, it is obtained:

$$15 \quad dU = C dT + \rho_w [L_f + (c_w - c_i)(T - T_{\text{ref}})] d\theta_w^{\text{ph}} + u_f d\theta_w^{\text{fl}} \quad (\text{B11})$$

where one can define:

$$dU^{\text{ph}} := C dT + \rho_w [L_f + (c_w - c_i)(T - T_{\text{ref}})] d\theta_w^{\text{ph}} \quad (\text{B12})$$

$$dU^{\text{fl}} := u_f d\theta_w^{\text{fl}} \quad (\text{B13})$$

20 The flux  $J$  is the heat advected by flowing water and equals to:

$$J = u_f \cdot J_w \quad (\text{B14})$$

Substituting Eqs. (B4) and (B13) in Eq. (B2) and considering that  $\nabla \bullet \mathbf{J} = u_f (\nabla \bullet \mathbf{J}_w)$  one obtains:

$$\frac{\partial U^{\text{ph}}}{\partial t} + \nabla \bullet \mathbf{G} + u_f \left( \frac{\partial \theta_w^{\text{fl}}}{\partial t} + \nabla \bullet \mathbf{J}_w \right) + S_{\text{en}} = 0 \quad (\text{B15})$$

From the second equation of (B6):

$$\frac{\partial \theta_w^{\text{fl}}}{\partial t} + \nabla \bullet \mathbf{J}_w = -S_w \quad (\text{B16})$$

Eventually Eq. (B15) becomes:

$$\frac{\partial U^{\text{ph}}}{\partial t} + \nabla \bullet \mathbf{G} + S_{\text{en}} - u_f S_w = 0 \quad (\text{B17})$$

## Appendix C

### Performance testing

As a demonstration of the performance of GEOtop with respect to snow, we use the data published by Morin et al. (2012) and drive the model with hourly measured near-surface meteorological data: air temperature, relative humidity, downwelling shortwave and longwave radiation, wind speed, air pressure and precipitation. The simulation was performed with standard parameters without improving the results by trial and error or fitting. An overview of the results (GEOtop-ColDePorte.pdf) as well as the parameter file used (GEOtop.inpts.ColDePorte) are available in Supplement. To demonstrate the performance with respect to topography, we used near-surface temperatures measured in steep bedrock that accumulates nearly no snow. The sites chosen for this demonstration are “Jungfrau ridge north” and “Jungfrau ridge south” (PERMOS,

## Simulating energy and water balance with freezing and terrain effects

S. Endrizzi et al.

Title Page

Abstract

Introduction

Conclusions

References

Tables

Figures

⏪

⏩

◀

▶

Back

Close

Full Screen / Esc

Printer-friendly Version

Interactive Discussion

2009). Horizon shading and sky view factor are parameterised based on fish-eye photography (Gruber et al., 2003). The simulations are driven by air temperature, relative humidity, wind speed, wind direction and global radiation from the SwissMetNet station Jungfraujoch. This driving station has a horizontal distance of about 1.2 km to the rock temperature measurements and is about 150 m lower in elevation. No snow cover is simulated. An overview of the results (GEOtop-JungfrauJoch.pdf) as well as the parameter file used (GEOtop.inpts.JungfrauJoch) are available in Supplement.

## Appendix D

### Distribution of meteorological data

10 In the GEOtop code a complete set of routines finalized at the spatial interpolations of meteorological variables is included. Air temperature is distributed according to Liston and Elder (2006a). All the measurements at different elevations are converted into values corresponding to a unique reference elevation according to a spatially constant lapse rate, which can however vary in time. The obtained values are spatially interpolated with the geostatistical method of Barnes (1964). On the interpolated temperature field, still referred to the reference elevation, the elevation correction given by the lapse rate multiplied by the difference between actual elevation and reference elevation, is applied. Relative humidity is converted into dew temperature, and the same interpolation method used for air temperature is used with a dew temperature lapse rate, which is normally smaller than the air temperature lapse rate (Liston and Elder, 2006a).

25 Wind speed is an important factor affecting the value of the fluxes. In order to describe the effect of topography on the surface energy balance it is important to consider in the model a topographically-dependent wind field. A full resolution of the fluid dynamic equations would be too computationally heavy for GEOtop. The wind field is instead parameterised using topography (Liston and Elder, 2006a). In particular, the

parameterisation is implemented correcting the wind speed with factors depending on slope and curvature of the surface:

$$w_s = w_{s0}(1 + c_s S + c_c C) \quad (D1)$$

where  $w_s$  is the wind speed modulus,  $w_{s0}$  the wind speed modulus ideally unaffected by topography,  $S$  the slope of the curve given by the intersection of the surface and by a vertical plane oriented in direction of the wind,  $C$  the curvature of the same curve, and  $c_s$  and  $c_c$  are calibration parameters. Wind direction is corrected according to Ryan (1977) in order to represent wind skirting round topographic obstacles.

Recently GEOTop has been also enabled to exploit MeteorIO (<http://models.slf.ch/p/meteoio/>), a library developed by the Snow and Avalanche Research institute of Davos (Switzerland) aimed at caching, filtering, resampling and spatial interpolating meteorological variables.

**Supplementary material related to this article is available online at <http://www.geosci-model-dev-discuss.net/6/6279/2013/gmdd-6-6279-2013-supplement.zip>.**

*Acknowledgements.* This study was funded through the nano-tera.ch project X-Sense. Model experiments were supported by the AAA/SWITCH funded Swiss Multi Science Computing Grid project ([www.smsg.ch](http://www.smsg.ch)) with computational infrastructure and support. Customized libraries (gGEOTop and GC3Pie) and user support were kindly provided by GC3: Grid Computing Competence Center ([www.gc3.uzh.ch](http://www.gc3.uzh.ch)). The International Foundation High Altitude Research Stations Jungfrauoch and Gornergrat supported field work for rock temperatures near Jungfrauoch. We acknowledge MeteoSwiss for providing driving climate time series at Corvatsch and Davos. Many people participated directly or indirectly in many development phases of GEOTop during the last decade. The keywords method actually used in GEOTop I/O had a first realisation with work of Emanuele Cordano; Glen Liston gave the code of his MicroMet model in FORTRAN from which derives the actual improved code used in GEOTop.

**Simulating energy and water balance with freezing and terrain effects**

S. Endrizzi et al.

Title Page

Abstract

Introduction

Conclusions

References

Tables

Figures



Back

Close

Full Screen / Esc

Printer-friendly Version

Interactive Discussion





## Simulating energy and water balance with freezing and terrain effects

S. Endrizzi et al.

Title Page

Abstract

Introduction

Conclusions

References

Tables

Figures

⏪

⏩

◀

▶

Back

Close

Full Screen / Esc

Printer-friendly Version

Interactive Discussion

- Brooks, R. H. and Corey, A. T.: Hydraulic properties of porous media, Hydrology paper, 3, Colorado State University, Fort Collins, 1964. 6305
- Brun, E., David, P., Sudul, M., and Brunot, G.: A numerical model to simulate snow-cover stratigraphy for operational avalanche forecasting, *J. Glaciol.*, 38, 13–22, 1992. 6281
- 5 Brutsaert, W.: On a derivable formula for long-wave radiation from clear skies, *Water Resour. Res.*, 11, 742–744, 1975a. 6294
- Brutsaert, W.: A theory for local evaporation (or heat transfer) from rough and smooth surfaces at ground level, *Water Resour. Res.*, 11, 543–550, 1975b. 6296
- Calonne, N., Flin, F., Morin, S., Lesaffre, B., du Roscoat, S. R., and Geindreau, C.: Numerical and experimental investigations of the effective thermal conductivity of snow, *Geophys. Res. Lett.*, 38, L23501, doi:10.1029/2011GL049234, 2011. 6302
- 10 Colbeck, S. C.: A theory of water percolation in snow, *J. Glaciol.*, 11, 369–385, 1972. 6305
- Cosenza, P., Guerin, R., and Tabbagh, A.: Relationship between thermal conductivity and water content of soils using numerical modelling, *Eur. J. Soil Sci.*, 54, 581–587, 2003. 6285, 6302
- 15 Crawford, T. M. and Duchon, C. E.: An improved parameterization for estimating effective atmospheric emissivity for use in calculating daytime downwelling longwave radiation, *J. Appl. Meteorol.*, 38, 474–480, 1998. 6295
- Daanen, R., Misra, D., and Epstein, H.: Active-layer hydrology in nonsorted circle ecosystems of the Arctic tundra, *Vadose Zone J.*, 6, 694–704, 2007. 6330
- 20 Dall’Amico, M., Endrizzi, S., Gruber, S., and Rigon, R.: A robust and energy-conserving model of freezing variably-saturated soil, *The Cryosphere*, 5, 469–484, doi:10.5194/tc-5-469-2011, 2011a. 6284, 6286, 6287, 6309, 6316, 6317
- Dall’Amico, M., Endrizzi, S., Gruber, S., and Rigon, R.: GEOtop Users Manual, Version 1.0, Technical report, Mountain-eering Srl, Siemensstr. 19 Bolzano, Italy, 2011b. 6315
- 25 De la Casiniere, A. C.: Heat exchange over a melting snow surface, *J. Glaciol.*, 13, 55–72, 1974. 6299
- de Vries, D. A.: Thermal properties of soil, in: *Physics of Plant Environment*, edited by: Van Wijk, W. R., North-Holland Publishing Co., Amsterdam, 210–235, 1963 6285
- Deardorff, J. W.: Efficient prediction of ground surface temperature and moisture with inclusion of a layer of vegetation, *J. Geophys. Res.*, 83, 1889–1903, 1978. 6295
- 30 Denby, B. and Greuell, W.: The use of bulk and profile methods for determining surface heat fluxes in the presence of glacier winds, *J. Glaciol.*, 46, 445–452, 2000. 6299

## Simulating energy and water balance with freezing and terrain effects

S. Endrizzi et al.

Title Page

Abstract

Introduction

Conclusions

References

Tables

Figures

⏪

⏩

◀

▶

Back

Close

Full Screen / Esc

Printer-friendly Version

Interactive Discussion

- Dickinson, R. E., Henderson-Sellers, A., and Kennedy, P. J.: Biosphere–Atmosphere Transfer Scheme (BATS) version 1e as coupled to the NCAR Community Land Model, Tech. rep., National Center for Atmospheric Research, Boulder, CO, USA, 1993. 6293
- Dilley, A. C. and O'Brien, D. M.: Estimating downward clear sky long-wave irradiance at the surface from screen temperature and precipitable water, *Q. J. Roy. Meteor. Soc.*, 124a, 1391–1401, 1997. 6294
- El-Mikkawy, M. and Karawia, A.: Inversion of general tridiagonal matrices, *Appl. Math. Lett.*, 19, 712–720, 2006. 6291
- Endrizzi, S. and Marsh, P.: Observations and modeling of turbulent fluxes during melt at the shrub-tundra transition zone 1: point scale variations, *Hydrol. Res.*, 41, 471–491, 2010. 6282, 6283
- Erbs, D. G., Klein, S. A., and Duffie, J. A.: Estimation of the diffuse radiation fraction for hourly, daily and monthly-average global radiation, *Sol. Energy*, 28, 293–302, 1982. 6297, 6298
- Flerchinger, G. N., Xaio, W., Marks, D., Sauer, T. J., and Yu, Q.: Comparison of algorithms for incoming atmospheric long-wave radiation, *Water Resour. Res.*, 45, W03423, doi:10.1029/2008WR007394, 2009. 6294
- Formetta, G., Mantilla, R., Franceschi, S., Antonello, A., and Rigon, R.: The JGrass-NewAge system for forecasting and managing the hydrological budgets at the basin scale: models of flow generation and propagation/routing, *Geosci. Model Dev.*, 4, 943–955, doi:10.5194/gmd-4-943-2011, 2011. 6282
- Formetta, G., Rigon, R., Chávez, J. L., and David, O.: Modeling shortwave solar radiation using the JGrass-NewAge system, *Geosci. Model Dev.*, 6, 915–928, doi:10.5194/gmd-6-915-2013, 2013. 6297
- Garen, D. C. and Marks, D.: Spatially distributed energy balance snowmelt modelling in a mountainous river basin: estimation of meteorological inputs and verification of model results, *J. Hydrol.*, 315, 126–153, 2005. 6306
- Garratt, J. R.: *The Atmospheric Boundary Layer*, Cambridge University Press, Cambridge, New York, Melbourne, 1992. 6296
- Gottardi, G. and Venutelli, M.: A control-volume finite-element model for two-dimensional overland flow, *Adv. Water Resour.*, 16, 277–284, 1993. 6289
- Gruber, S., Peter, M., Hoelzle, M., Woodhatch, I., and Haeberli, W.: Surface temperatures in steep alpine rock faces – a strategy for regional-scale measurement and modelling, in:

## Simulating energy and water balance with freezing and terrain effects

S. Endrizzi et al.

Title Page

Abstract

Introduction

Conclusions

References

Tables

Figures

⏪

⏩

◀

▶

Back

Close

Full Screen / Esc

Printer-friendly Version

Interactive Discussion

Proceedings of the 8th International Conference on Permafrost, 21–25 July 2003, Zurich, Switzerland, 1, 325–330, 2003. 6319

Gruber, S., Hoelzle, M., and Haeberli, W.: Rock-wall temperatures in the Alps: modelling their topographic distribution and regional differences, *Permafrost Periglac.*, 15, 299–307, 2004. 6286

Gubler, S., Gruber, S., and Purves, R. S.: Uncertainties of parameterized surface downward clear-sky shortwave and all-sky longwave radiation., *Atmos. Chem. Phys.*, 12, 5077–5098, doi:10.5194/acp-12-5077-2012, 2012. 6294, 6295

Gubler, S., Endrizzi, S., Gruber, S., and Purves, R. S.: Sensitivities and uncertainties of modeled ground temperatures in mountain environments, *Geosci. Model Dev.*, 6, 1319–1336, doi:10.5194/gmd-6-1319-2013, 2013. 6310, 6315

Halberstam, I. and Schieldge, J. P.: Anomalous behavior of the atmospheric surface layer over a melting snowpack, *J. Appl. Met.*, 20, 255–265, 1981. 6299

Hansson, K., Simunek, J., Mizoguchi, M., Lundin, L., and van Genuchten, M.: Water flow and heat transport in frozen soil numerical solution and freeze-thaw applications, *Vadose Zone J.*, 3, 693–704, 2004. 6288, 6330

Helbig, N., Löwe, H., and Lehning, M.: Radiosity approach for the shortwave surface radiation balance in complex terrain, *J. Atmos. Sci.*, 66, 2900–2912, 2009. 6298

Hinzman, L. D., Goering, D. J., and Kane, D. L.: A distributed thermal model for calculating soil temperature profiles and depth of thaw in permafrost regions, *J. Geophys. Res.*, 103, 975–991, 1998. 6330

Hock, R.: Temperature index melt modelling in mountain areas, *J. Hydrol.*, 282, 104–115, 2003. 6294

Horton, P., Schaefli, B., Mezghani, A., Hingray, B., and Musy, A.: Assessment of climate-change impacts on alpine discharge regimes with climate model uncertainty, *Hydrol. Process.*, 20, 2091–2109, 2006. 6282

Houghton, H. G.: On the annual heat balance of the northern hemisphere, *J. Meteorol.*, 11, 1–9, 1954. 6293

Idso, S. B.: A set of equations for full spectrum and 8 to 14  $\mu\text{m}$  and 10.5 to 12.5  $\mu\text{m}$  thermal radiation from cloudless skies, *Water Resour. Res.*, 17, 295–304, 1981. 6294

Iqbal, M.: *An Introduction to Solar Radiation*, Academic Press, Toronto, 1983. 6292

## Simulating energy and water balance with freezing and terrain effects

S. Endrizzi et al.

Title Page

Abstract

Introduction

Conclusions

References

Tables

Figures

⏪

⏩

◀

▶

Back

Close

Full Screen / Esc

Printer-friendly Version

Interactive Discussion

- Ivanov, V. Y., Vivoni, E. R., Bras, R. L., and Entekhabi, D.: Catchment hydrologic response with a fully distributed triangulated irregular network model, *Water Resour. Res.*, 40, 1–23, 2004. 6282
- Johansen, O.: Thermal conductivity of soils, Ph.D. thesis, Norwegian Technical University, Trondheim, 1975. 6285
- Jordan, R.: A one-dimensional temperature model for a snow cover: Technical documentation for SNTHERM 89, Tech. rep., US Army Cold Regions Research and Engineering Laboratory, Hanover, NH, USA, 1991. 6300, 6301, 6302, 6305
- Jordan, R., Andreas, E. L., and Makshtas, A. P.: Heat budget of snow-covered sea ice at North Pole 4, *J. Geophys. Res.*, 104, 7785–7806, 1999. 6302, 6303, 6307
- Kelley, C.: Solving Nonlinear Equations with Newton's Method, Society for Industrial Mathematics, Philadelphia, 2003. 6282, 6291
- Kienzie, S. W.: A new temperature based method to separate rain and snow, *Hydrol. Process.*, 22, 5067–5085, 2008. 6306
- Konzelmann, T., van de Wal, R. S. W., Greuell, W., Bintanja, R., Henneken, E. A. C., and Abe-Ouchi, A.: Parameterization of global and longwave incoming radiation for the Greenland Ice Sheet, *Global Planet. Change*, 9, 143–164, 1994. 6294
- Koopmans, R. W. R. and Miller, R. D.: Soil freezing and soil water characteristic curves, *Soil Sci. Soc. Am. J.*, 30, 680–685, 1966. 6285
- Kuchment, L. S., Gelfan, A. N., and Demidov, V. N.: A distributed model of runoff generation in the permafrost regions, *J. Hydrol.*, 240, 1–22, 2000. 6330
- Kurylyk, B. and Watanabe, K.: The mathematical representation of freezing and thawing processes in variably-saturated, non-deformable soils, *Adv. Water Resour.*, 60, 160–177, 2013. 6288
- Lehning, M., Völksch, I., Gustafsson, D., Nguyen, T., Stähli, M., and Zappa, M.: ALPINE3D: a detailed model of mountain surface processes and its application to snow hydrology, *Hydrol. Process.*, 20, 2111–2128, 2006. 6281, 6330
- Liang, X., Lettenmaier, D. P., Wood, E. F., and Burges, S. J.: A simple hydrologically based model of land surface water and energy fluxes for general circulation models, *J. Geophys. Res.-Atmos.*, 99, 14415–14428, 1994. 6282
- Liston, G. E. and Elder, K.: A meteorological distribution system for high-resolution terrestrial modeling (MicroMet), *J. Hydrometeorol.*, 11, 217–234, 2006a. 6319



## Simulating energy and water balance with freezing and terrain effects

S. Endrizzi et al.

Title Page

Abstract

Introduction

Conclusions

References

Tables

Figures

⏪

⏩

◀

▶

Back

Close

Full Screen / Esc

Printer-friendly Version

Interactive Discussion

- description of the Community Land Model (CLM), Tech. Rep. NCAR/TN-461+STR, National Center for Atmospheric Research, Boulder, CO, USA, 2004. 6330
- Painter, S. L.: Three-phase numerical model of water migration in partially frozen geological media: model formulation, validation, and applications, *Comput. Geosci.*, 15, 69–85, 2011. 6330
- Panday, S. and Huyakorn, P.: A fully coupled physically-based spatially-distributed model for evaluating surface/subsurface flow, *Adv. Water Resour.*, 27, 361–382, 2004. 6284
- Paniconi, C. and Putti, M.: A comparison of Picard and Newton iteration in the numerical solution of multidimensional variably saturated flow problems, *Water Resour. Res.*, 30, 3357–3374, 1994. 6281
- Panofsky, H. A. and Dutton, J. A.: *Atmospheric Turbulence Models and Methods for Engineering Applications*, John Wiley and Sons, New York, 1984. 6296
- PERMOS: Permafrost in Switzerland 2004/2005 and 2005/2006, in: *Glaciological Report (Permafrost) No. 6/7 of the Cryospheric Commission of the Swiss Academy of Sciences*, edited by: Nötzli, J. and Vonder Mühll, D., University of Zurich, 2009. 6318
- Prata, A. J.: A new long-wave formula for estimating downward clearsky radiation at the surface, *Q. J. Roy. Meteor. Soc.*, 122, 1127–1151, 1996. 6294
- Rigon, R., Bertoldi, G., and Over, T. M.: GEOtop: a distributed hydrological model with coupled water and energy budgets, *J. Hydrometeorol.*, 7, 371–388, 2006. 6281
- Ryan, B. C.: A mathematical model for diagnosis and prediction of surface winds in mountainous terrain, *J. Appl. Meteorol.*, 16, 571–584, 1977. 6320
- Satterlund, D. R.: An improved equation for estimating longwave radiation from the atmosphere, *Water Resour. Res.*, 15, 1649–1650, 1979. 6294
- Shimizu, H.: *Air Permeability of Deposited Snow*, vol. 22, Institute of Low Temperature Science, Sapporo, Japan, 1970. 6306
- Sicart, J. E., Pomeroy, J. W., Essery, R. L. H., and Bewley, D.: Incoming longwave radiation to melting snow: observations, sensitivity and estimation in northern environments, *Hydrol. Process.*, 20, 3697–3708, 2006. 6295
- Snyder, W. C., Wan, Z., Zhang, Y., and Feng, Y.-Z.: Classification-based emissivity for land surface temperature measurement from space, *Int. J. Remote Sens.*, 19, 2753–2774, 1998. 6295
- Spaans, E. and Baker, J.: The soil freezing characteristic: its measurement and similarity to the soil moisture characteristic, *Soil Sci. Soc. Am. J.*, 60, 13–19, 1996. 6285

## Simulating energy and water balance with freezing and terrain effects

S. Endrizzi et al.

Title Page

Abstract

Introduction

Conclusions

References

Tables

Figures

⏪

⏩

◀

▶

Back

Close

Full Screen / Esc

Printer-friendly Version

Interactive Discussion

- Sturm, M., Holmgren, J., König, M., and Morris, K.: The thermal conductivity of seasonal snow, *J. Glaciol.*, 43, 26–41, 1997. 6302
- Tarboton, D. G. and Luce, C. H.: Utah energy balance snow accumulation and melt model (UEB), Tech. rep., Utah Water Research Laboratory, Utah State University and USDA Forest Service Intermountain Research Station, Logan, Utah, 1996. 6294
- 5 Therrien, R. and Sudicky, E.: Three-dimensional analysis of variably-saturated flow and solute transport in discretely-fractured porous media, *J. Contam. Hydrol.*, 23, 1–44, 1996. 6281
- US Army Corps of Engineers: Snow hydrology, Summary report of the snow investigations, Tech. rep., US Army Corps of Engineers, North Pacific Division, Portland, OR, USA, 1956. 6306
- 10 Van Der Vorst, H. A.: BI-CGSTAB: A fast and smoothly converging variant of BI-CGSTAB for the solution of nonsymmetric linear systems, *SIAM J. Sci. Stat. Comput.*, 13, 631–644, 1992. 6291
- Van Genuchten, M. T.: A closed-form equation for predicting the hydraulic conductivity of unsaturated soils., *Soil Sci. Soc. Am. J.*, 44, 892–898, 1980. 6286, 6288, 6331
- VanderKwaak, J. E. and Loague, K.: Hydrologic-Response simulations for the R-5 catchment with a comprehensive physics-based model, *Water Resour. Res.*, 37, 999–1013, 2001. 6281
- Vionnet, V., Brun, E., Morin, S., Boone, A., Faroux, S., Le Moigne, P., Martin, E., and Willemet, J.-M.: The detailed snowpack scheme Crocus and its implementation in SURFEX v7.2, *Geosci. Model Dev.*, 5, 773–791, doi:10.5194/gmd-5-773-2012, 2012. 6309, 6310
- 20 Wagnon, P., Ribstein, P., Kaser, G., and Berton, P.: Energy balance and runoff seasonality of a Bolivian glacier, *Global Planet. Change*, 22, 49–58, 1999. 6299
- Wettlaufer, J. S. and Worster, M. G.: Premelting dynamics, *Annu. Rev. Fluid Mech.*, 38, 427–452, 2006. 6285
- 25 Ye, Z. and Pielke, R. A.: Atmospheric parameterization of evaporation from non-plant-covered surfaces, *J. Appl. Meteorol.*, 32, 1248–1258, 1993. 6296
- Yen, Y.: Review of thermal properties of snow, ice and sea ice, Tech. Rep. 81–10, Cold Regions Research and Engineering Laboratory, Hanover, NH, USA, 1981. 6302
- Zanotti, F., Endrizzi, S., Bertoldi, G., and Rigon, R.: The GEOTOP snow module, *Hydrol. Process.*, 18, 3667–3679, 2004. 6283
- 30 Zehe, E., Maurer, T., Ihringer, J., and Plate, E.: Modeling water flow and mass transport in a loess catchment, *Phys. Chem. Earth Pt. B*, 26, 487–507, 2001. 6281

Zhang, Z., Kane, D. L., and Hinzman, L. D.: Development and application of a spatially-distributed Arctic hydrological and thermal process model (ARHYTHM), *Hydrol. Proces.*, 14, 1017–1044, 2000. 6330

## GMDD

6, 6279–6341, 2013

### Simulating energy and water balance with freezing and terrain effects

S. Endrizzi et al.

Title Page

Abstract

Introduction

Conclusions

References

Tables

Figures



Back

Close

Full Screen / Esc

Printer-friendly Version

Interactive Discussion



## Simulating energy and water balance with freezing and terrain effects

S. Endrizzi et al.

**Table 1.** Overview of existing simulators dealing with soil freezing processes. Abbreviations: in the snow column: dd = degree day factor, ly = one-layer energy balance, mly = multilayer energy balance; in the soil energy and water balance columns: 0d = simplified, 1d = one-dimensional (vertical) solution of the heat or Richards equation, 3d = three-dimensional solution; in the column about the energy exchange with atmosphere: wiT = with complex topography, woT = without complex topography.

Model	Snow	Soil energy balance	Soil water balance	Energy exchange with atmosphere	Discharge
Hinzman et al. (1998)		1d		woT	
Oleson et al. (2004)	mly	1d	1d	woT	yes
Lehning et al. (2006)	mly	1d	0d	wiT	yes
Marchenko et al. (2008)	mly	1d		woT	
Kuchment et al. (2000)	dd	1d	0d	woT	yes
Zhang et al. (2000)	ly	0d	0d	woT	yes
McKenzie et al. (2007)		3d	3d		yes
Daanen et al. (2007)		3d	3d		
Hansson et al. (2004)		3d	3d		yes
Painter (2011)		3d	3d		
GEOtop	mly	1d	3d	wiT	yes

Title Page

Abstract

Introduction

Conclusions

References

Tables

Figures

⏪

⏩

◀

▶

Back

Close

Full Screen / Esc

Printer-friendly Version

Interactive Discussion

## Simulating energy and water balance with freezing and terrain effects

S. Endrizzi et al.

Title Page

Abstract

Introduction

Conclusions

References

Tables

Figures

⏪

⏩

◀

▶

Back

Close

Full Screen / Esc

Printer-friendly Version

Interactive Discussion

**Table 2.** Table of symbols for soil balance and overland flow equations.

Symbol	Name	Value or Range	Unit
$t$	time		s
$T$	temperature		°C
$\rho_w$	density of liquid water in soil	1000	kg m <sup>-3</sup>
$\rho_i$	density of ice	918	kg m <sup>-3</sup>
$\rho_{sp}$	density of soil particles		kg m <sup>-3</sup>
$\theta_w$	fraction of liquid water in soil		dimensionless
$\theta_i$	fraction of ice in soil		dimensionless
$z_f$	elevation with respect to a reference		m
$z_0$	elevation at the soil surface		m
$z$	position in the soil column along the vertical		m
$\Delta z_l$	depth of the cell /		m
$g$	gravity acceleration	9.81	ms <sup>-2</sup>
$\theta_a$	fraction of air or gaseous components in the soil		dimensionless
$\theta_{sp}$	soil saturated water content (soil porosity)		dimensionless
$\theta_r$	residual water content		dimensionless
$\Theta_v$	$\theta_w + \theta_i$		dimensionless
$\Theta_m$	$\theta_w + \frac{\rho_i}{\rho_w} \theta_i$		dimensionless
$\psi_{w0}$	soil matric potential corresponding to $\Theta_v$		m
$\psi$	liquid water pressure head		m
$\psi_T$	soil matric potential resulting from the generalized Clapeyron Equation		m
$T_m$	water melting temperature at atmospheric pressure	273.15	K
$T^*$	depressed water melting temperature under unsaturated conditions		K
$T_{ref}$	reference temperature, usually set to $T_m$		K
$\alpha$	parameter according to Van Genuchten (1980)		mm <sup>-1</sup>
$n$	parameter according to Van Genuchten (1980)		dimensionless
$m$	parameter according to Van Genuchten (1980)	usually: $m := 1 - n^{-1}$	dimensionless
$J_w$	volumetric liquid water flux		ms <sup>-1</sup>

## Simulating energy and water balance with freezing and terrain effects

S. Endrizzi et al.

**Table 2.** Continued.

Symbol	Name	Value or Range	Unit
$K$	hydraulic conductivity		$\text{ms}^{-1}$
$k_s$	conductance		$\text{ms}^{-1}$
$\lambda_T$	total thermal conductivity of soil		$\text{Wm}^{-1}\text{K}^{-1}$
$\lambda_{\text{sp}}$	thermal conductivity of the soil grains		$\text{Wm}^{-1}\text{K}^{-1}$
$\lambda_w$	water thermal conductivity	0.6	$\text{Wm}^{-1}\text{K}^{-1}$
$\lambda_i$	ice thermal conductivity	2.29	$\text{Wm}^{-1}\text{K}^{-1}$
$\lambda_a$	air thermal conductivity	2.29	$\text{Wm}^{-1}\text{K}^{-1}$
$L_f$	latent heat of fusion	333.7	$\text{kJkg}^{-1}$
$\gamma$	coefficient in the conductance formulation		dimensionless
$C$	total volumetric thermal capacity of soil		$\text{Jm}^{-3}\text{K}^{-1}$
$C_a$	volumetric apparent thermal capacity of soil		$\text{Jm}^{-3}\text{K}^{-1}$
$c_i$	specific thermal capacity of ice	2117	$\text{Jkg}^{-1}\text{K}^{-1}$
$c_w$	specific thermal capacity of water	4188	$\text{Jkg}^{-1}\text{K}^{-1}$
$c_{\text{sp}}$	specific thermal capacity of soil particles		$\text{Jkg}^{-1}\text{K}^{-1}$
$c_s$	soil surface roughness coefficient		$\text{m}^{1-\gamma}\text{s}^{-1}$
$P_e$	effective precipitation		$\text{ms}^{-1}$
$U$	volumetric internal energy of soil		$\text{Jm}^{-3}$
$s$	length along the direction of maximum slope		m
$S_{\text{en}}$	sink term of energy losses		$\text{Wm}^{-3}$
$S_w$	sink term of mass losses		$\text{s}^{-1}$
$G$	heat conduction flux in the ground		$\text{Wm}^{-2}$
$J$	heat flux due to water advection		$\text{Wm}^{-2}$

Title Page

Abstract

Introduction

Conclusions

References

Tables

Figures

⏪

⏩

◀

▶

Back

Close

Full Screen / Esc

Printer-friendly Version

Interactive Discussion

**Table 3.** Table of symbols for the atmospheric variables.

Symbol	Name	Value or Range	Unit
$SW_{in}$	incoming shortwave radiation		$W m^{-2}$
$SW_{out}$	outgoing shortwave radiation		$W m^{-2}$
$SW_{toa}$	shortwave radiation at top of atmosphere		$W m^{-2}$
$LW_{in}$	incoming longwave radiation		$W m^{-2}$
$LW_{out}$	outgoing longwave radiation		$W m^{-2}$
$H$	sensible heat flux		$W m^{-2}$
$LE$	latent heat flux		$W m^{-2}$
$LW_{out}$	outgoing longwave radiation		$W m^{-2}$
$Q_{sur}^*$	saturated air specific humidity at the surface		$kg kg^{-1}$
$Q_a$	specific air humidity		$kg kg^{-1}$
$r_a$	aerodynamic resistance		dimensionless
$L_e$	specific heat of evaporization		$J kg^{-1}$
$\alpha_Y$	coefficient taking account the soil resistance to evaporation		dimensionless
$\beta_Y$	coefficient taking account the soil resistance to evaporation		dimensionless
$\rho_a$	air density		$kg m^{-3}$
$c_p$	specific heat at constant pressure		$kg m^{-3}$
$\rho_a$	air density		$kg m^{-3}$
$\tau_a$	atmospheric transmissivity		dimensionless
$\tau_c$	cloud transmissivity		dimensionless
$\tau_R$	transmissivity for Rayleigh scattering		dimensionless
$\tau_g$	gas absorption transmissivity		dimensionless
$\tau_w$	water vapor transmissivity		dimensionless
$\tau_{aer}$	aerosols transmissivity		dimensionless
$\epsilon_a$	atmosphere emissivity		dimensionless
$\epsilon_c$	cloudy emissivity		dimensionless
$e_a$	water vapour pressure		bar
$\sigma$	Stefan–Boltzmann constant	$5.67 \times 10^8$	$W m^{-2} K^{-4}$
$c$	cloud fraction		dimensionless
$p$	air pressure		bar
$T_a$	air temperature		$^{\circ}C$
$T_{sur}$	surface temperature		$^{\circ}C$
$T_{sur,K}$	surface temperature		K
$w_s$	wind speed		$ms^{-1}$

## Simulating energy and water balance with freezing and terrain effects

S. Endrizzi et al.

**Table 4.** Table of symbols for the snow.

Symbol	Name	Value or Range	Unit
$U_s$	volumetric internal energy of snow		$\text{J m}^{-3}$
$\theta_{ws}$	fraction of liquid water in snow		dimensionless
$\theta_{is}$	fraction of ice in snow		dimensionless
$S_e$	effective saturation		dimensionless
$S_r$	irreducible water saturation		dimensionless
$K_s$	snow hydraulic conductivity		$\text{m s}^{-1}$
$P_s$	weight of overlying snow column		Pa
$T_s$	snow temperature		$^{\circ}\text{C}$
$D$	snow layer height		m
$\phi_s$	snow porosity		dimensionless
$C_1$	compaction rate (destructive metamorphism)		$\text{s}^{-1}$
$C_2$	compaction rate (overburden)		$\text{s}^{-1}$
$\eta$	snow viscosity		$\text{N s m}^{-2}$
$J_{ws}$	water flux in snow		$\text{m s}^{-1}$
$\rho_{ns}$	density of new snow		$\text{kg m}^{-3}$
$M_{\text{tot}}$	mass per unit surface of the whole snowpack		$\text{kg m}^{-2}$
$M_{\text{up}}^*$	max mass per unit surface of the upper region		$\text{kg m}^{-2}$
$M_{\text{dw}}^*$	max mass per unit surface of the lower region		$\text{kg m}^{-2}$
$M_1^*$	max mass per unit surface admitted for a layer		$\text{kg m}^{-2}$
$M_l$	mass per unit surface of a layer		$\text{kg m}^{-2}$
$N_{\text{mid}}^*$	max number of layers admitted for the middle region		dimensionless
$N_{\text{mid}}$	number of layers of the middle region		dimensionless

Title Page

Abstract

Introduction

Conclusions

References

Tables

Figures

⏪

⏩

◀

▶

Back

Close

Full Screen / Esc

Printer-friendly Version

Interactive Discussion

## Simulating energy and water balance with freezing and terrain effects

S. Endrizzi et al.

**Table 5.** Definition of snow discretisation regions.

Case	Upper	Middle	Bottom
$0 < M_{\text{tot}} \leq M_{\text{up}}^*$	X	/	/
$M_{\text{up}}^* < M_{\text{tot}} \leq M_{\text{up}}^* + M_{\text{dw}}^*$	X	/	X
$M_{\text{tot}} > M_{\text{up}}^* + M_{\text{dw}}^*$	X	X	X

Title Page

Abstract

Introduction

Conclusions

References

Tables

Figures

⏪

⏩

◀

▶

Back

Close

Full Screen / Esc

Printer-friendly Version

Interactive Discussion

## Simulating energy and water balance with freezing and terrain effects

S. Endrizzi et al.

Title Page

Abstract

Introduction

Conclusions

References

Tables

Figures



Back

Close

Full Screen / Esc

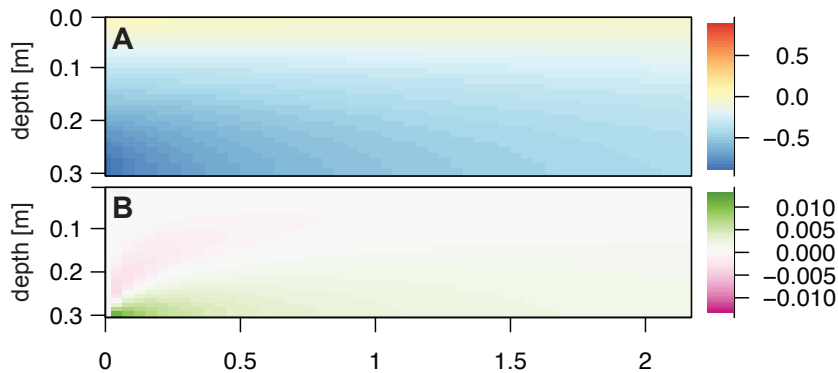
Printer-friendly Version

Interactive Discussion

**Table 6.** Available processes in a layer and triggering condition.

Operation	Region	Triggering condition
layer splitting	upper region	$\rho_{\text{ns}}D > M_1^*$
layers merging	middle region	new snow and $N_{\text{mid}} > N_{\text{mid}}^*$
layers merging	all	melting in one time step

## Temperature and temperature differences [°C]



## Total water content and total water content differences [-]

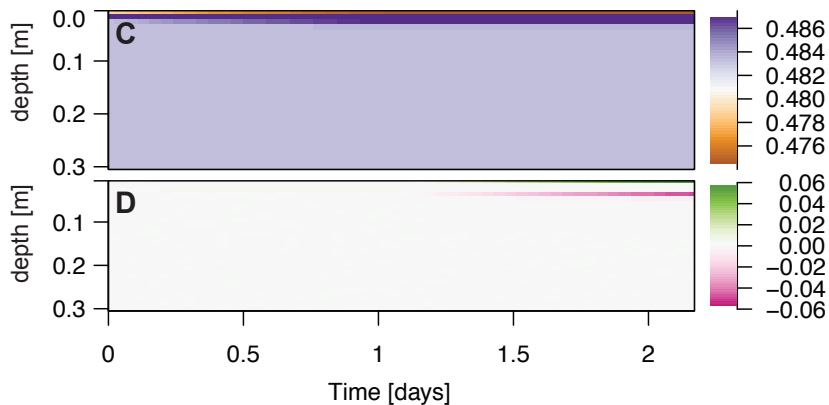


**Fig. 1.** Evolution of temperature (**A**) and total water content (**C**) for simulations with a time step of 1 s. The difference to the solutions with a time step of 1 h are also shown for temperature (**B**) and total water content (**D**) based on subtracting the hourly solution from the 1 s solution.

## Simulating energy and water balance with freezing and terrain effects

S. Endrizzi et al.

cell size: 20 meters

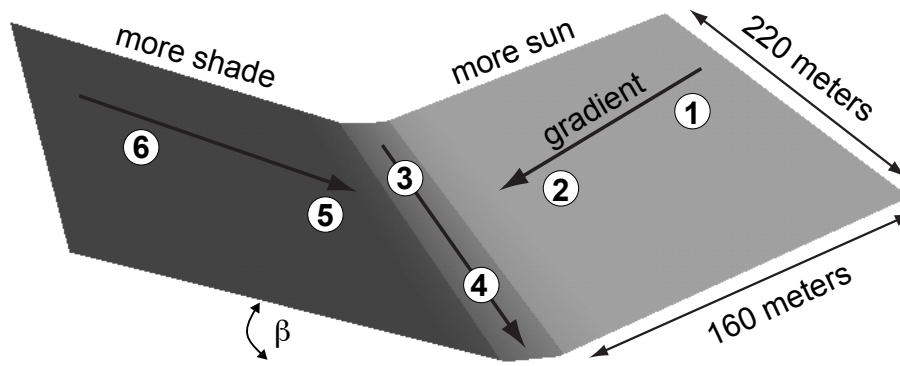


**Fig. 2.** Synthetic catchment and location of points analysed. The converging topography has a sun-exposed and a more shaded side. It is varied with respect to the inclination angle of its hillslopes  $\beta$ . Channel inclination, in the direction from point 3 to 4, is always  $5^\circ$ .

Title Page

Abstract

Introduction

Conclusions

References

Tables

Figures

◀

▶

◀

▶

Back

Close

Full Screen / Esc

Printer-friendly Version

Interactive Discussion

## Simulating energy and water balance with freezing and terrain effects

S. Endrizzi et al.

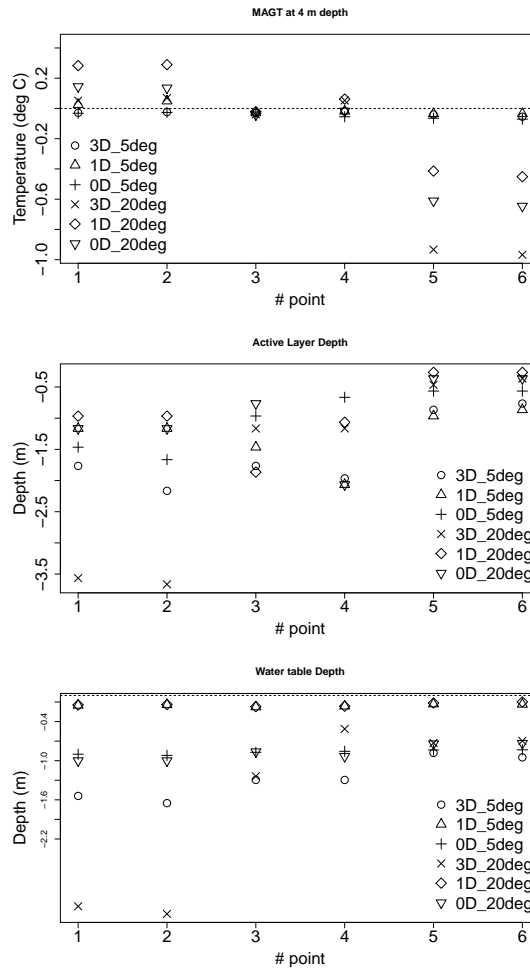


**Fig. 3.** Mean annual ground temperature at a 4 m depth, active layer depth, and water table depth for the six points shown in Fig. 2 given by the six simulations that have been performed.

[Title Page](#)  
[Abstract](#)   [Introduction](#)  
[Conclusions](#)   [References](#)  
[Tables](#)   [Figures](#)  
⏪   ⏩  
◀   ▶  
[Back](#)   [Close](#)  
[Full Screen / Esc](#)  
[Printer-friendly Version](#)  
[Interactive Discussion](#)



## Simulating energy and water balance with freezing and terrain effects

S. Endrizzi et al.

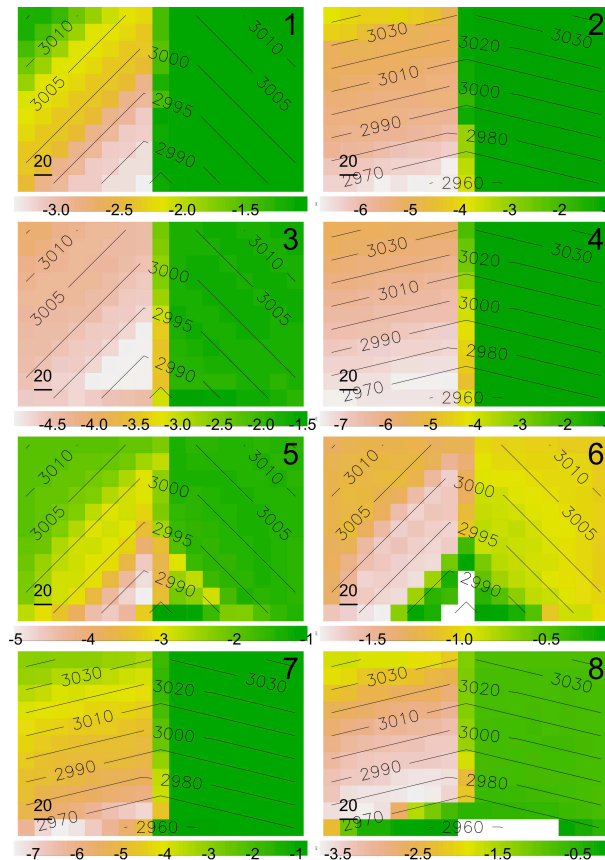


**Fig. 4.** Distributed results: active layer depth for the simulations 5° 0-D (1), 20° 0-D (2), 5° 1-D (3), 20° 1-D (4), active layer depth (5) and mean annual water table depth (in metres) (6) for the simulation 5° 3-D, and active layer depth (7) and mean annual water table depth (8) for the simulation 20° 3-D. All depths and the scale are in metres, and the elevations in m.a.s.l.

Title Page

Abstract

Introduction

Conclusions

References

Tables

Figures

◀

▶

◀

▶

Back

Close

Full Screen / Esc

Printer-friendly Version

Interactive Discussion

## Simulating energy and water balance with freezing and terrain effects

S. Endrizzi et al.

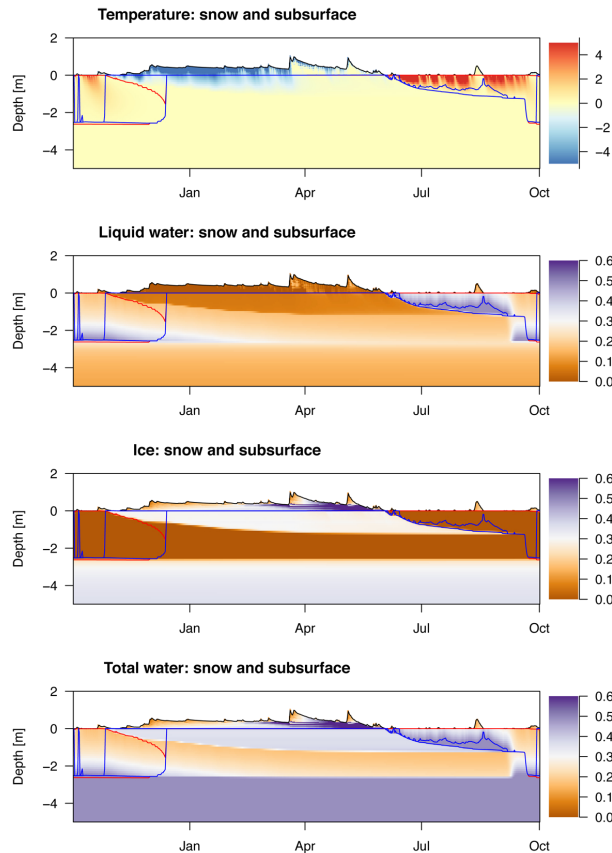


**Fig. 5.** Time evolution of temperature, and liquid, solid, and total water content for soil and snow in Point 1, as shown in Fig. 2, for the simulation for the 5° topography 3-D. The blue line indicates the water table, while the lower and upper borders of the thawed layer are shown in red. Negative depths correspond to soil, and positive depths to the snow cover.

[Title Page](#)[Abstract](#)[Introduction](#)[Conclusions](#)[References](#)[Tables](#)[Figures](#)[⏪](#)[⏩](#)[◀](#)[▶](#)[Back](#)[Close](#)[Full Screen / Esc](#)[Printer-friendly Version](#)[Interactive Discussion](#)